NAVAL POSTGRADUATE SCHOOL
Monterey, California

THESIS

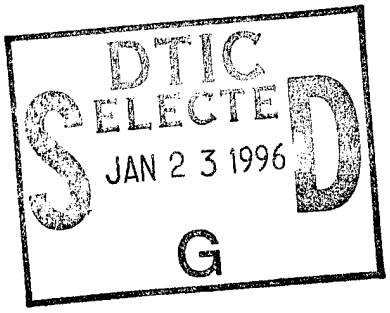

AN ANALYSIS OF DATA COMPRESSION ALGORITHMS USED IN THE TRANSMISSION OF IMAGERY

by

Mark A. Sanford

June, 1995

Thesis Advisors: Kyle T. Alfriend
Nicholas D. Beser

Approved for public release; distribution is unlimited.

REPORT DOCUMENTATION PAGE

Form Approved
OMB No. 0704-0188

1. AGENCY USE ONLY *(Leave blank)*	2. REPORT DATE June 1995	3. REPORT TYPE AND DATES COVERED Master's Thesis

4. TITLE AND SUBTITLE: AN ANALYSIS OF DATA COMPRESSION ALGORITHMS USED IN THE TRANSMISSION OF IMAGERY

5. FUNDING NUMBERS

6. AUTHOR(S) Mark A. Sanford

7. PERFORMING ORGANIZATION NAME(S) AND ADDRESS(ES)
Naval Postgraduate School
Monterey CA 93943-5000

8. PERFORMING ORGANIZATION REPORT NUMBER

9. SPONSORING/MONITORING AGENCY NAME(S) AND ADDRESS(ES)

10. SPONSORING/MONITORING AGENCY REPORT NUMBER

11. SUPPLEMENTARY NOTES The views expressed in this thesis are those of the author and do not reflect the official policy or position of the Department of Defense or the U.S. Government.

12a. DISTRIBUTION/AVAILABILITY STATEMENT Approved for public release; distribution unlimited

12b. DISTRIBUTION CODE

13. ABSTRACT *(maximum 200 words)*

In the tactical arena, the timely receipt of imagery is of highest priority. Lossy compression of the imagery for transmission increases the ability to provide imagery in a timely fashion. In the reconstruction of this imagery, some distortion is acceptable as long as the ability to extract relevant information is retained. This thesis is an independent assessment of four image compression algorithms (Joint Photographic Experts Group (JPEG) compression, Wavelet Compression, Fractal Compression and the compression algorithm contained in the Navy TENCAP sponsored Radiant Tin Program) for their ability to provide an imagery product of sufficient quality which meets the requirements of tactical users.

The quantitative analysis shows that most quantitative measures are not useful for rating compression methods. In the qualitative assessment, using the Analytic Hierarchy Process, Wavelet compression appears to be the best choice of compression method across the various compression ratios. JPEG does very well at low ratios of compression as expected. Similarly, the Radiant Tin algorithm does very well at high ratios of compression. In the application of tactical imagery, fractal compression does not seem to be a good choice.

14. SUBJECT TERMS
Data Compression, Image Compression, Imagery, Wavelets, Fractals, JPEG, Radiant Tin

15. NUMBER OF PAGES
125

16. PRICE CODE

17. SECURITY CLASSIFICATION OF REPORT	18. SECURITY CLASSIFICATION OF THIS PAGE	19. SECURITY CLASSIFICATION OF ABSTRACT	20. LIMITATION OF ABSTRACT
Unclassified	Unclassified	Unclassified	UL

NSN 7540-01-280-5500

Standard Form 298 (Rev. 2-89)
Prescribed by ANSI Std. 239-18

Approved for public release; distribution is unlimited.

AN ANALYSIS OF DATA COMPRESSION ALGORITHMS USED IN THE TRANSMISSION OF IMAGERY

Mark A. Sanford
Lieutenant, United States Navy
B.S., Villanova University, 1986

Submitted in partial fulfillment of the
requirements for the degree of

**MASTER OF SCIENCE IN SYSTEMS TECHNOLOGY
(SPACE SYSTEMS OPERATIONS)**

from the

NAVAL POSTGRADUATE SCHOOL
June 1995

Author: Mark A. Sanford
Mark A. Sanford

Approved by: Kyle T. Alfriend, Thesis Advisor
Kyle T. Alfriend, Thesis Advisor

Nicholas D. Beser, Thesis Advisor

Rudolf Panholzer, Chairman,
Space Systems Academic Group

ABSTRACT

In the tactical arena, the timely receipt of imagery is of highest priority. Lossy compression of the imagery for transmission increases the ability to provide imagery in a timely fashion. In the reconstruction of this imagery, some distortion is acceptable as long as the ability to extract relevant information is retained. This thesis is an independent assessment of four image compression algorithms (Joint Photographic Experts Group (JPEG) Compression, Wavelet Compression, Fractal Compression and the compression algorithm contained in the Navy TENCAP sponsored Radiant Tin Program) for their ability to provide an imagery product of sufficient quality which meets the requirements of tactical users.

The quantitative analysis shows that most quantitative measures are not useful for rating compression methods. In the qualitative assessment, using the Analytic Hierarchy Process, Wavelet Compression appears to be the best choice of compression method across the various compression ratios. JPEG does very well at low ratios of compression as expected. Similarly, the Radiant Tin algorithm does very well at high ratios of compression. In the application of tactical imagery, Fractal Compression does not seem to be a good choice.

TABLE OF CONTENTS

ACKNOWLEDGMENT

I would like to thank the following people for the assistance they provided in the preparation of this thesis.

- Dr. Terry Alfriend and Dr. Nick Beser, my advisors, for their patience, advice and guidance in preparing this thesis.
- Jim Happel, Will Geckle and John Florence of the Johns Hopkins University, Applied Physics Laboratory for their critique of the subjective evaluation used for this experiment.
- Dr. Bruce Hammell of the Johns Hopkins University Applied Physics Laboratory for his expert advice on setting-up a psychological experiment.
- The Radiant Tin team at the Johns Hopkins University Applied Physics Laboratory and the NPS Space Systems Operations (SO-41) students who participated in the qualitative experiment used for this thesis.
- Mr. Joel Maloney and the staff at the National Photographic Interpretation Center for their assistance in choosing the imagery used for the qualitative experiment.
- The Radiant Tin team at Texas Tech University for their assistance in clarifying the details on the Radiant Tin algorithm.

I. INTRODUCTION

A. THE NEED FOR IMAGE COMPRESSION

Today's tactical commander must make better decisions faster than ever before. One of the resources the commander can use to aid in these decisions is imagery. Imagery can provide information regarding enemy troop strength and movement, the enemy industrial base, terrain mapping for deployment of Marines and Special Forces, Battle Damage Assessment and weather over intended targets. Technology has essentially placed this imagery and more at the commander's fingertips. The increased use of imagery, by a variety of users reaching down to the individual Sailor/Marine/soldier/airman in the field has precipitated the need for image compression.

Imagery comes from a variety of sources ranging from large space-based collectors to hand-held digital cameras carried by a SEAL team or Marine reconnaissance unit. Imagery collected from space-based resources is useful for both scientific and tactical purposes. Scientific uses of imagery collected from space based sensors include remote sensing of the earth and its atmosphere and interplanetary exploration missions such as Voyager, the Mars Observer, Clementine and Galileo. Inherent to scientific research, a tight level of control over error is required so that results are not distorted.

Images require large numbers of bits to represent them digitally. For example, a small SPOT image, which is 5196 pixels x 5196 pixels, using 8 bits per pixel requires 2.16×10^8 bits or approximately 27 Megabytes to represent the image (Internet SPOT page). A modest number of images can quickly take up the hard disk capacity of the typical personal computer.

In the tactical arena, imagery from both space-based collectors and other sources is potentially useful to the tactical commander. The essential problem with tactical uses of imagery is that of timeliness. Images for tactical applications require high data rate and high bandwidth communications for transmission in their uncompressed form in a timely manner. This is particularly important for the tactical commander who requires some forms of imagery in near real-time. Additionally, disadvantaged users, (such as

submarines, SEAL teams and Marine Reconnaissance Units), are exposed for too long a time to transmit substantial amounts of imagery. As such, image compression has become increasingly important to meet these requirements.

B. WHAT IS IMAGE COMPRESSION?

Image compression is the means of encoding a data stream, representing an image, using a reduced number of bits. All image compression/decompression systems contain two basic parts, an encoder and a decoder (Figure 1.1). The encoder may encode the data using a lossy or a lossless algorithm.

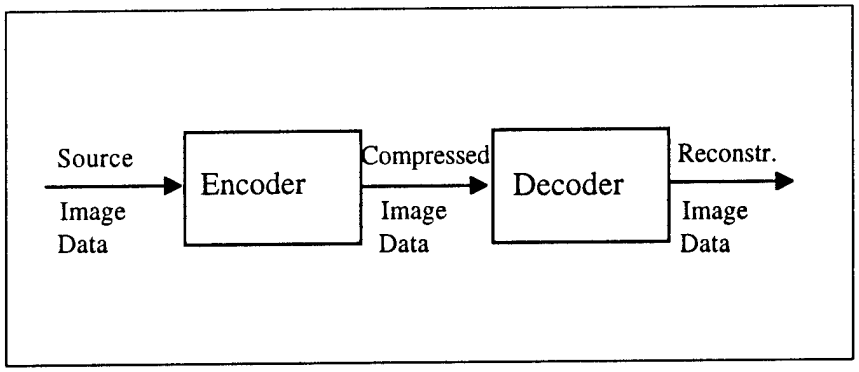

Figure 1.1 Generic Image Compression System (Pennebaker and Mitchell, p. 66)

Inherent to each image is some amount of redundant information. Lossless compression algorithms encode this redundancy in a smaller number of bits than were used in the original image. The reconstructed image is numerically identical to the original image on a pixel-by-pixel basis. (Rabbani, p.6). Lossy compression not only compresses the redundant information but also compresses some of the unique information in the image. The reconstructed image is then an approximation of the original image. (Rabbani, p.6). While the difference between the reconstructed and original images may possibly be statistically significant, the interpretability of the image may not suffer. Figure 1.2 describes graphically the difference between lossless and lossy compression as well as a graphical explanation of the compression ratio. The goal of lossy compression then is to design a compression algorithm where the errors in the reconstructed image are not critical to the exploitation of information from the image.

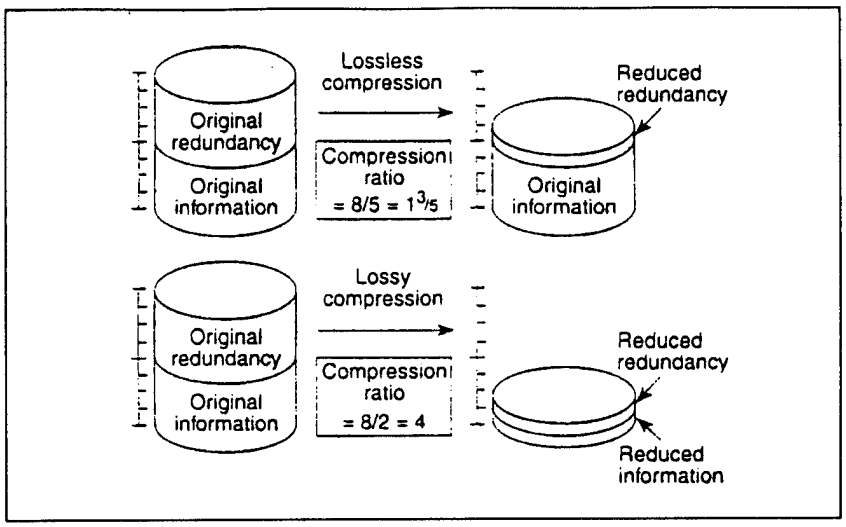

Figure 1.2 Relationship between lossless and lossy compression and the compression ratio (Beser, p. 210)

While lossless imagery may be the ideal, it is generally not practical since the lossless algorithm is driven by the information rate (discussed in Chapter II), and, the compression ratios are typically low. Additionally, this translates into a larger data set requiring more time and larger bandwidth to transmit. As such, some differences in the reconstructed image are usually acceptable to provide the time of response required and to satisfy bandwidth constraints. Therefore, lossy compression is the prevalent means of compressing tactical imagery.

C. PURPOSE

Research work in image compression is very popular, particularly as the "information highway" continues to expand. Similarly, imagery has taken on an increasingly important role in all facets of military strategy and planning. In the tactical arena, timeliness of the imagery is of highest priority. Lossy compression of the imagery for transmission increases the ability to provide imagery in a timely fashion. In the reconstruction of this imagery, some distortion is acceptable as long as the ability to extract relevant information is retained. This thesis provides an independent assessment of four image compression algorithms for their ability to provide an imagery product of sufficient quality to meet the requirements of tactical users.

D. THESIS LAYOUT

Chapter II discusses the fundamentals of image compression along with basic definitions. Chapter III contains a survey of the four methods of image compression that will be examined in this thesis:

- International Standards Organization Joint Photographic Experts Group (ISO-JPEG) Compression;
- Wavelet Compression;
- Fractal Compression; and
- Navy TENCAP's Radiant Tin.

The criteria used for the selection of tactical imagery and the tactical applications for imagery are discussed in Chapter IV. A survey of image compression quality measures is contained in Chapter V. This survey will include a discussion of both subjective and quantitative measures. Chapter VI contains an analysis of the ability of each of the four compression methods to satisfactorily compress imagery for tactical uses. The results of the analysis are contained in Chapter VII. Additionally, recommendations are provided that detail when each method is appropriate for use based on the ability to extract tactical information from the reconstructed image.

II. IMAGE COMPRESSION FUNDAMENTALS

The lossy compression of imagery is performed in a three step process. This process is shown in Figure 2.1.

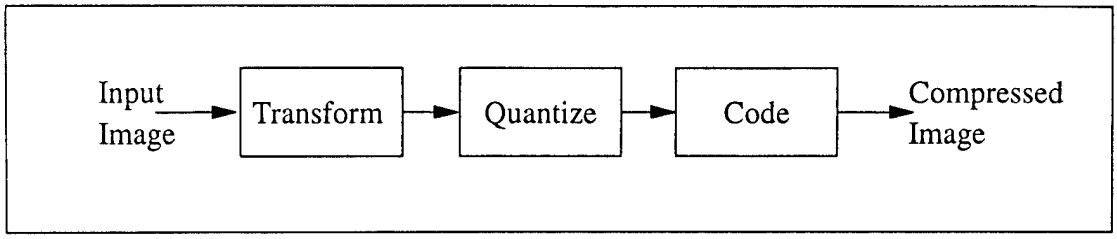

Figure 2.1 Generic Image Compression Algorithm

Lossless algorithms follow a similar process eliminating the quantizing step. This chapter will take each step and describe it in a generic manner so that the discussion of particular compression algorithms in Chapter III may draw on this background.

A. TRANSFORMATION

The transform coding process is designed to take an N x N pixel image and to divide it into n x n smaller blocks. Each of these blocks is then processed using a unitary transform. A unitary transform being a "reversible linear transform whose kernel describes a set of complete, orthonormal discrete basis functions (Rabbani, p. 102)." This serves to redistribute the signal energy into just a few coefficients. The other coefficients can either be discarded in the quantization step or can be very efficiently coded using lossless means. The unitary transform step may be viewed in one of two fashions; as Coordinate Axes Rotations or as Basis Function Decompositions.

1. Coordinate Axes Rotation

Generally, adjacent pixel values are highly correlated. If the original image is subdivided into 1 x 2 pixel blocks, each of these vectors would represents a pair of adjacent pixels. If each of these pixel pairs were plotted in a 2-dimensional coordinate system (x_1 , x_2) the majority of the points would lie on the 45° diagonal defined by $x_1 = x_2$. The variance defined along the direction x_j ,where j=1,2, is defined as:

(1) $\sigma_{x_j}^2 = \frac{1}{M}\sum_{i=1}^{M}(x_{ji} - x_j)^2$ *(Rabbani, p. 103)*

where M is the total number of blocks in the image and $\overline{x_j}$ is the mean value of x_j over all blocks. (Rabbani, p. 103) Unfortunately, the variance is large in both the x_1 and x_2 directions (this is shown in Figure 2.2) and as such, if either x_1 or x_2 is encoded as the corresponding mean, large reconstruction errors (Mean Squared Error) will result.

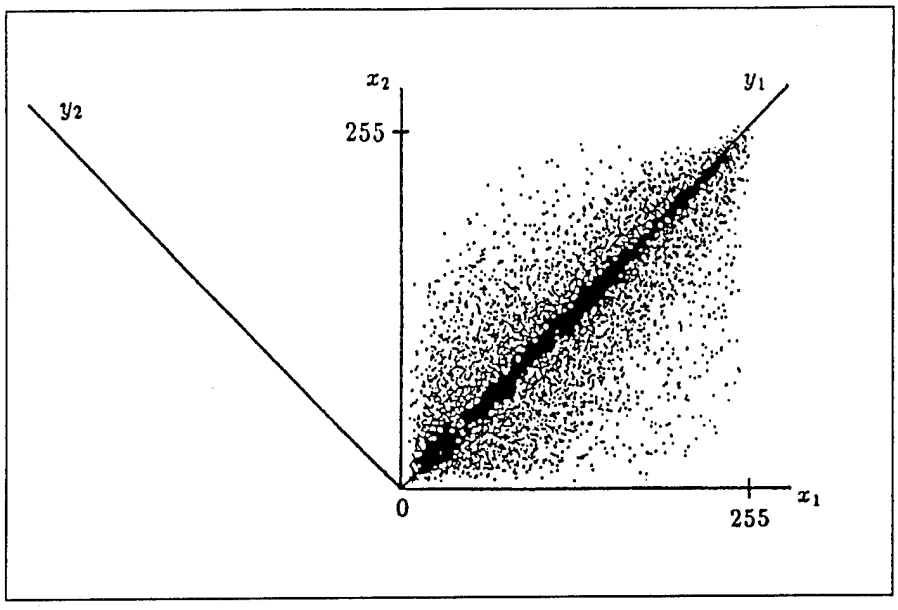

Figure 2.2 Example of a Rotation Transform (Rabbani, p. 104)

If, however, each of these vectors is rotated to a new set of axes (y_1 , y_2) in the following manner:

(2) $$\begin{bmatrix} y_1 \\ y_2 \end{bmatrix} = \frac{1}{\sqrt{2}}\begin{bmatrix} 1 & 1 \\ -1 & 1 \end{bmatrix}\begin{bmatrix} x_1 \\ x_2 \end{bmatrix}$$ *(Rabbani, p. 104)*

In matrix notation:

(3) $\boldsymbol{Y = AX}$

A is the rotation matrix with equation 3 defining the forward transform. Upon decoding on the receive end, the inverse transform will restore the original data. The inverse transform is defined as:

(4) $$\begin{bmatrix} x_1 \\ x_2 \end{bmatrix} = \frac{1}{\sqrt{2}} \begin{bmatrix} 1 & -1 \\ 1 & 1 \end{bmatrix} \begin{bmatrix} y_1 \\ y_2 \end{bmatrix}$$ *(Rabbani, p. 105)*

or alternately as:

(5) $\mathbf{X=BY}$ *where* $\mathbf{B=A^{-1}}$

In the original orientation $\sigma_{x_1}^2 \approx \sigma_{x_2}^2$. However in the transformed orientation $\sigma_{y_1}^2 >> \sigma_{y_2}^2$ and as such, if y_2 is replaced with its mean value (being 0) the mean squared error which results ($\sigma_{y_2}^2$) is significantly smaller than either $\sigma_{x_1}^2$ or $\sigma_{x_2}^2$. Now that many of the coefficients are 0 (i.e., contain little energy) they can be efficiently coded using the methods described in Section D. (Rabbani, p. 105)

2. Basis Function Decomposition

Using equation 5 above leads to the viewing of transforms as Basis Function Decompositions. The columns of the **B** matrix can be seen as discrete orthogonal basis functions. These basis functions when weighted by the **Y** matrix and added together return the original data matrix **X**. Each type of image transform has it's own set of basis functions. These functions can be used as elementary components in representing an image, given the corresponding transform coefficients. (Rabbani, p. 106)

B. TYPES OF TRANSFORMATION CODING

1. Frequency Transformation

There are several methods of frequency transformation, two of which are often described in the literature: the Discrete Fourier Transform (DFT) and the Discrete Cosine Transform. As the DFT is generally used for spectral analysis and filtering, only the Discrete Cosine Transform will be discussed. Descriptions of the DFT as well as other methods may be found in the references.

The Discrete Cosine Transform (DCT) is a classic example of transformation. The N x N image is first divided into n x n blocks. Each block is then placed through the Forward Discrete Cosine Transform which is defined as:

(6) $$F(u,v) = \frac{4C(u)C(v)}{n^2} \sum_{j=0}^{n-1} \sum_{k=0}^{n-1} f(j,k) \cos\left[\frac{(2j+1)u\pi}{2n}\right] \cos\left[\frac{(2k+1)v\pi}{2n}\right]$$ *(Rabbani, p. 108)*

where u and v are the horizontal and vertical indices of the transformed block and j and k being the horizontal and vertical indices of the original block. F(u,v) is the pixel value at the position u,v in the transformed block and f(j,k) is the pixel value at the position j,k in the original block. C(u) and C(v) are defined as:

(7) $\frac{1}{\sqrt{2}}$ for u,v = 0 and 1 otherwise

An example of this transform using an 8 x 8 sub-block is shown in Tables 2.1 and 2.2. Table 2.1 is the original block, while Table 2.2 is the transformed block.

	j=0	j=1	j=2	j=3	j=4	j=5	j=6	j=7
k=0	139	144	149	153	155	155	155	155
k=1	144	151	153	156	159	156	156	156
k=2	150	155	160	163	158	156	156	156
k=3	159	161	162	160	160	159	159	159
k=4	159	160	161	162	162	155	155	155
k=5	161	161	161	161	160	157	157	157
k=6	162	162	161	163	162	157	157	157
k=7	162	162	161	161	163	158	158	158

Table 2.1 Original 8 x 8 Image Block (Rabbani, p. 116)

	u=0	u=1	u=2	u=3	u=4	u=5	u=6	u=7
v=0	315	0	-3	-1	1	-1	-1	0
v=1	-6	-4	-2	-1	-1	0	0	0
v=2	-3	-2	-1	1	0	0	0	0
v=3	-2	-1	0	0	0	0	0	0
v=4	0	0	0	1	0	0	0	0
v=5	1	0	1	0	0	0	0	0
v=6	0	0	0	0	0	1	0	0
v=7	-1	1	1	-1	1	0	0	0

Table 2.2 Transformed 8 x 8 Block

The Inverse Discrete Cosine Transform is defined as:

(8) $$f(j,k) = \sum_{u=0}^{n-1} \sum_{v=0}^{n-1} C(u)C(v)F(u,v) \cos\left[\frac{(2j+1)u\pi}{2n}\right] \cos\left[\frac{(2k+1)v\pi}{2n}\right]$$ *(Rabbani, p. 108)*

F(u,v), f(j,k), C(u), and C(v) are defined as above.

Upon application of the Inverse DCT, the pixel values in the original block are restored.

2. Other Types of Transformation

There are several other types of algorithms. These transforms are not transforms in the sense of the previous definition, however, they still change the data in some fashion so that it may be coded in an efficient manner.

a. Spatial Transformation

Spatial transformation is based on the fact that there is a high correlation between adjacent pixels in a typical image. Spatial transformation uses predictive coding techniques which use this statistic to their advantage. The most common spatial transformation technique is Differential Pulse Code Modulation.

There are two versions of Differential Pulse Code Modulation (DPCM), lossy and lossless. Both algorithms use the same transformation step. Each pixel is predicted using an m-order predictor. This means that there are m pixels used in a linear combination to form the predictor. A difference image is then created which is made up of the differences between the pixel value and its predictor. Typically, a single-predictor is used for the entire image. For the following example, the 3rd order predictor 0.75A-0.5B+.75C is used. A is the value to the left of the pixel to be predicted, B is the value to the upper left and C is the value above the pixel to be predicted.

139	144	149	153
144	151	153	156
150	155	160	163
159	161	162	160

Table 2.3 Original Pixel Block

0	0	0	0
0	146.5	153	155
0	153.75	155.5	160.5
0	160.5	163.25	163.75

Table 2.4 Pixel Predictors for the Pixels in Table 2.3

139	144	149	153
144	4.5	0	1
150	1.25	4.5	2.5
159	0.5	-1.25	-3.75

Table 2.5 Difference Image

The difference image (with the exception of those coefficients in the first row and column which are transmitted separately) will change the image statistics from an arbitrary distribution to a Laplacian Distribution with mean of zero. (Figure 2.3)

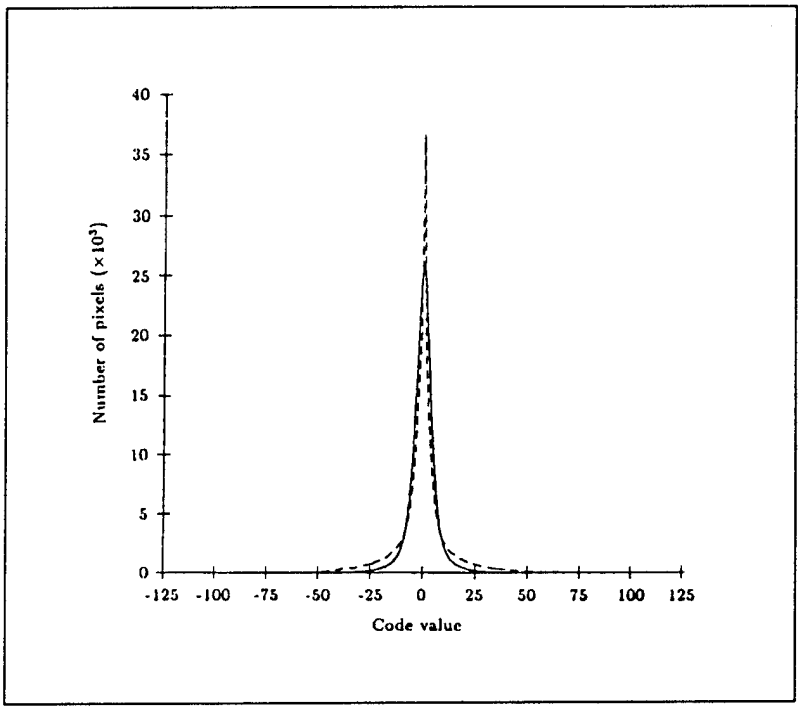

Figure 2.3 Differential Image Histogram (Rabbani, p. 61)

Lossless coding of the differential image is then done using the methods described in Section D. Lossy coding of the differential image is done by first quantizing the values in the difference image (Section C) and then coding using the methods in Section D.

b. Symbolic Transformation

Symbolic transformation is an innovative technique that is particularly useful in imagery containing man-made objects. The image is converted from its original pixel space representation to a symbol space representation. This conversion extracts features

such as edges, arcs and textures and then converts them into symbols. These symbols are then coded separately from the background. Upon receipt and restoration of the background of the image, the symbols are then decoded and replaced in the image. The Radiant Tin algorithm is an example of symbolic transformation and is explained in Chapter III.

C. QUANTIZATION

Quantizers are staircase functions that take a variety of input values and map them into a finite number of output values. Quantizers may be based on either statistical or human visual system characteristics. Two methods of quantization will be discussed: the Lloyd-Max Quantization and Vector Quantization. Other methods may be found in the references.

1. Lloyd-Max Quantizer

The Lloyd-Max quantizer is based on minimizing the Mean Square Error between the original and quantized values. The quantizer maps the original values (from possibly a continuous source) into discrete "quantized" values termed reconstruction levels. The range of values that are mapped into these reconstruction levels are termed decision levels. (Rabbani, p. 84)

The derivation of the Lloyd-Max quantizer is based on minimizing the following equation on both d (the decision levels) and r (the reconstruction levels).

$$(9) \qquad D = \sum_{i=0}^{N-1} \int_{d_i}^{d_{i+1}} (e - r_i)^2 p_e(e) de \quad \textit{(Rabbani, p. 84)}$$

e is the differential image and $p_e(e)$ is the distribution of the pixel values to be quantized.

The solution gives decision levels "halfway between the neighboring reconstruction levels and reconstruction levels that lie at the center of the mass of the probability density enclosed by the two adjacent decision levels." The mathematical solution to this is:

$$(10) \qquad d_i = \frac{r_{i-1} + r_i}{2} \quad \textit{(Rabbani, p. 84)}$$

$$(11) \quad r_i = \frac{\int_{d_i}^{d_{i+1}} e p_e(e) de}{\int_{d_i}^{d_{i+1}} P_e(e) de} \quad \textit{(Rabbani, p. 84)}$$

Typically these equations will not yield closed-form solutions and must be solved using numerical techniques. In some circumstances (such as a Laplacian probability density function) a closed form solution does exist. Given a Laplacian density and a 3-bit quantizer the decision and reconstruction levels are listed in Table 2.6 and shown in Figure 2.4.

i	$(d_i, d_{i+1}) \rightarrow r_i$	Probability
0	$(-255, -16) \rightarrow -20$	0.025
1	$(-16, -8) \rightarrow -11$	0.047
2	$(-8, -4) \rightarrow -6$	0.145
3	$(-4, 0) \rightarrow -2$	0.278
4	$(0, 4) \rightarrow 2$	0.283
5	$(4, 8) \rightarrow 6$	0.151
6	$(8, 16) \rightarrow 11$	0.049
7	$(16, 255) \rightarrow 20$	0.022

Table 2.6 8-level Lloyd-Max Quantizer (Rabbani, p. 86)

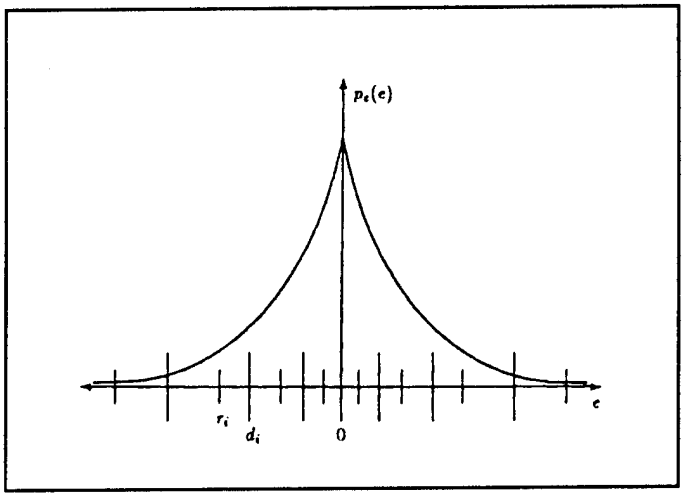

Figure 2.4 8 level Lloyd-Max Quantizer (Rabbani, p. 86)

2. Vector Quantization

Vector quantization is based on the use of a predetermined codebook for encoding. The image is first divided into fixed size vectors of pixels. These vectors are then compared against the codebook The index of the vector is then transmitted which is where the compression is realized. The key to this technique is "training" the codebook. This "training" involves processing a variety of test imagery that best represents the imagery that will be compressed. From this test imagery, the codebook of vectors that represent the most common vectors is generated. While several algorithms have been-used, the Linde-Buzo-Gray algorithm is the generally accepted algorithm. In-depth discussion of Vector Quantization may be found in the references. (Rabbani, p. 145)

D. CODING

The coding step is where the compression of the data stream actually occurs. The amount of compression is based on the entropy of the data stream. Entropy being the amount of original (i.e., non-redundant) information in the data stream. Shannon defined entropy as:

$$(12) \quad Entropy = -\sum_{i=0}^{L-1} p_i \log_2 p_i \quad bits\ per\ symbol$$

In lossless coding methods, each symbol is encoded with a number of bits that equals or exceeds the entropy. In lossy coding methods, each symbol is encoded with fewer bits than the entropy.

1. Entropy Coding

a. Huffman Coding

Huffman Coding is a variable length code. It is based on giving the characters with the higher probability of occurrence the shorter code, and those with lower probabilities of occurrence the longer code. There are two basic restrictions placed on the formation of the code; first, no two characters will consist of identical codes and second, each code will be constructed such that no additional indication is necessary to specify where a code begins and ends once the starting point is known (Huffman, p. 1098).

The procedure for generating the Huffman code is relatively simple and is diagrammed in Figure 2.5.

- Stage 1: The two free nodes with the lowest frequency are located. A parent node is created by assigning a weight equal to the sum of the two child nodes. The left most child node is given a "0" code and the right most node is given a "1" code. (Step 1 in Figure 2.5)
- Stage 2: The parent node then replaces the two child nodes and Step 1 is repeated until only one free node remains. (Steps 2 - 4 in Figure 2.5)

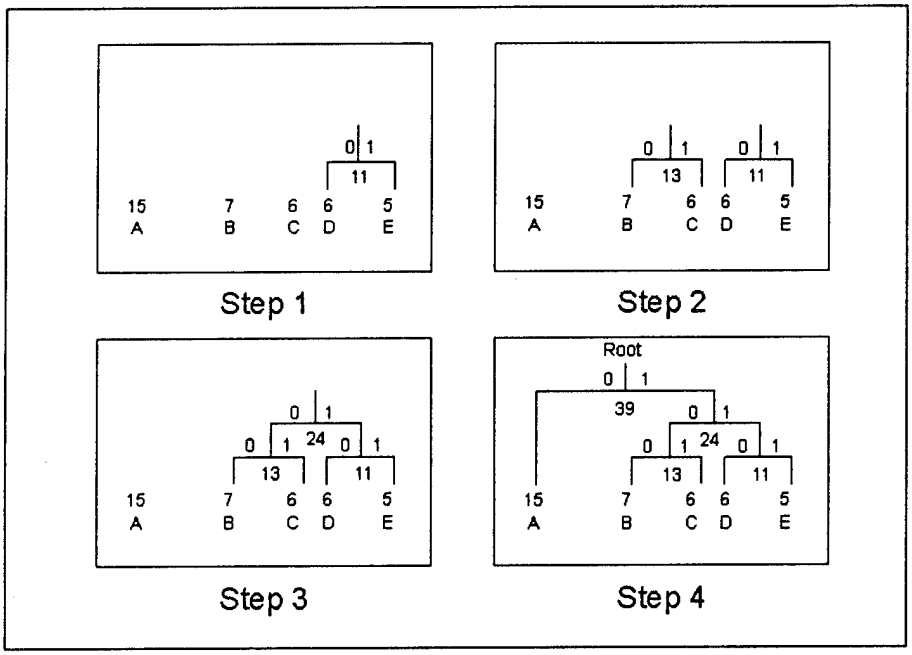

Figure 2.5 Pictorial Representation of Huffman Coding (Beser)

This results in the following coding scheme:

Symbol	Code
A	0
B	100
C	101
D	110
E	111

Table 2.7 Huffman Coding Scheme (Beser)

Decoding a given bit stream is relatively simple. Given a starting point, the bit stream is followed until a recognized code is found. Once found, the process is repeated

until the stream is decoded. For example, using the above coding scheme and the bit stream 11011101101010100, from left to right the stream would be decoded into:

110 111 0 110 101 0 100

D E A D C A B (Beser).

b. Arithmetic Coding

The process of arithmetic coding is relatively simple. It begins with a particular data "message" that is represented on the interval [0,1). As each symbol is coded the interval used to represent it becomes smaller as its bit representation grows. The symbols with smaller probabilities of occurrence reduce the interval substantially while the symbols with greater probability of occurrence reduce the interval by small amounts. The process is best shown by an example. (Witten, Neal and Cleary, p. 521)

The encoding process begins with the interval being initialized to [0,1). For this example the following probabilities will be used:

Symbol	Probability	Range
a	0.2	[0, 0.2)
e	0.3	[0.2. 0.5)
i	0.1	[0.5, 0.6)
o	0.2	[0.6, 0.8)
u	0.1	[0.8, 0.9)
!	0.1	[0.9, 1.0)

Table 2.8 Example Probability Distribution of Symbols (Witten, Neal, Cleary p, 521)

To encode the message eaii!

The interval [0,1) is divided into 6 pieces, with each piece corresponding proportionally to the probabilities in Table 2.8. Since the first character to be encoded is an e, the interval becomes [0.2, 0.5). This interval is then subdivided into pieces corresponding again to the probabilities above. The second character reduces the interval to [0.2, 0.26). The process is continued until the entire string is coded with the final interval being [0.23354, 0.2336). The step by step process is shown in Table 2.9. (Witten, Neal and Cleary, p. 522)

Symbol	Low	High
	0	1
e	0.2	0.5
a	0.2	0.26
i	0.23	0.236
i	0.233	0.2336
!	0.23354	0.2336

Table 2.9 Example Arithmetic Coding Steps (Witten, Neal and Cleary, p. 522)

Then encoding process can be summed up by the following piece of code:

```
low = 0.0;
high = 1.0;
while ((c=getc(input))!=EOF){
        range = high - low;
        high  = low + range*high_range(c);
        low   = low + range*low_range(c);
}
output(low);  (Nelson, p. 126)
```

The decoding process is also simple. The following code showing the decoding algorithm (end-of-string not being a consideration):

```
number = input_code();
for(;;){
        symbol=find_symbol_straddling_this_range(number);
        putc(symbol);
        range = high_range(symbol) - low_range(symbol);
        number = number - low_range(symbol);
        number = number/range;
} (Nelson, p.127)
```

The decode algorithm only requires 1 of the 2 sides of the interval for decoding. The message string from above would then be decoded step by step as follows:

Number	Output Symbol	Low	High	Range
0.23354	e	0.2	0.5	0.3
0.1118	a	0	0.2	0.2
0.559	i	0.5	0.6	0.1
0.59	i	0.5	0.6	0.1
0.9	!	0.9	1	0.1
0				

Table 2.10 Example Arithmetic Decoding Steps (Witten, Neal and Cleary, p. 522)

c. Run-length Coding

Run-length coding is designed to take advantage of redundancies in the data stream. Images with a high level of neighboring pixel correlation will achieve high ratios of compression, those with low levels of correlation will achieve, at worst, no compression. The coding is accomplished by simply counting the number of repeating symbols and replacing them with the symbol and the count. For example the string "aaabcddddddeefggggg" would be encoded as 3a, b, c, 6d, 2e, f, 5g.

d. Zerotree Coding

Zerotree Coding is one of the newest coding methods. As this scheme was designed for use in Wavelet compression, it will be discussed in Chapter III.

2. Sub-band Coding

Subband coding is the process where image data is filtered into a number of images. Each of the resulting images contains only a particular band of frequencies from the original image, thus the term subband. Each subband contains a reduced bandwidth compared to the original image. The subbands used in Wavelet compression techniques are the result of a two-dimensional, four band analysis bank shown in Figure 2.6.

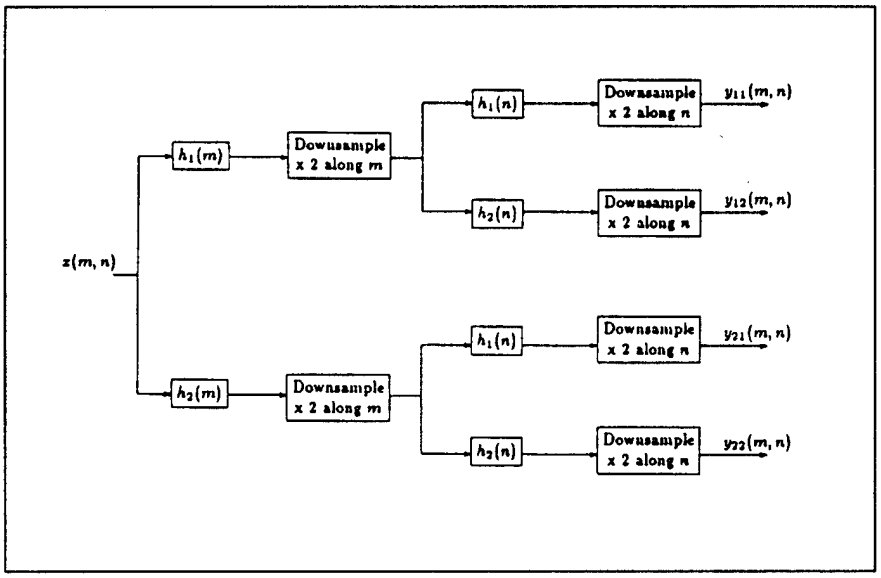

Figure 2.6 2-D, four-band analysis bank (Rabbani, p. 174)

The image is first placed through a high pass and a low pass filter. Each of the resulting images is also placed through the same high pass and low pass filters. The resulting four subbands, the result of the two-dimensional four-band analysis bank, the image in Figure 2.7 results.

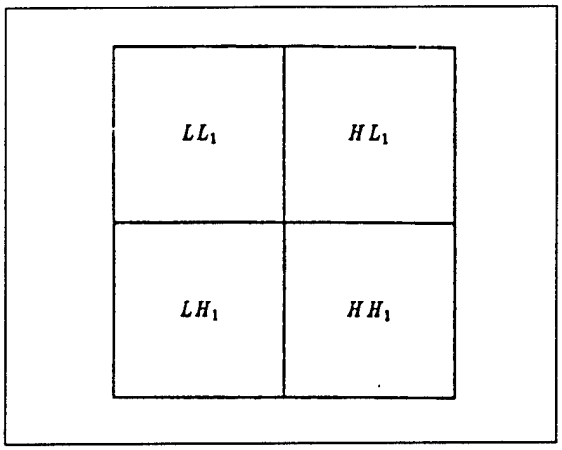

Figure 2.7 One pass through the 2-D four-band analysis bank (Shapiro, p. 3447)

Additional passes of the LL_1 subband through the analysis bank may be done to further separate the subbands. This is shown in Figure 2.8.

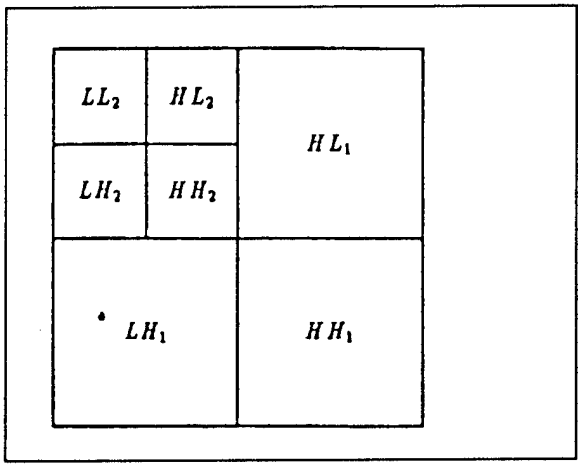

Figure 2.8 Results after passing the LL_1 subband through the analysis bank (Shapiro, p. 3447)

The Low Pass/Low Pass subband (LL) is a reduced resolution representation of the original image. Once the subbands have been established, the coefficients can then be quantized and coded using the methods discussed above.

III. IMAGE COMPRESSION ALGORITHM OVERVIEW

This chapter contains an overview of the four data compression methods that are analyzed in this thesis: International Standards Organization Joint Photographic Experts Group (ISO-JPEG), Wavelet Compression, Fractal Compression and the compression algorithm contained in the Navy TENCAP Radiant Tin Program (hereafter referred to as Radiant Tin compression). The basic methodology behind each algorithm is provided as a background. Detailed discussion of the algorithms may be found in the references.

These particular methods were chosen for a variety of reasons. ISO-JPEG was chosen as it is one of the compression algorithms selected by the National Imagery Transmission Format Board for inclusion in their software and is formally documented in the ISO Draft International Standard 10918 Part 1 (MIL-STD 188-198A, p.1). Wavelet compression was chosen since the Central Imagery Office (CIO) is currently considering its use for their low entropy compression requirements. Fractal compression was chosen as it is used for compression of weather imagery and also as it is being investigated for use on some Navy projects. Finally, Radiant Tin was chosen for its specific design to handle and process tactical imagery at high ratios of compression.

A. JOINT PHOTOGRAPHIC EXPERTS GROUP (JPEG)

The International Organization for Standardization (ISO), the International Telegraph and Telephone Consultative Committee (CCITT) and the International Electrotechnical Commission (IEC) created the Joint Photographic Experts Group (JPEG) to establish an international standard for image compression. The JPEG is a working group made up of members from the three organizations. The JPEG standard consists of four modes for compression of imagery: a baseline algorithm (sequential Discrete Cosine Transform), a sequential lossless algorithm, a progressive DCT algorithm and a hierarchical algorithm which uses elements from each of the other three methods. Figure 3.1 shows the relationship between the modes.

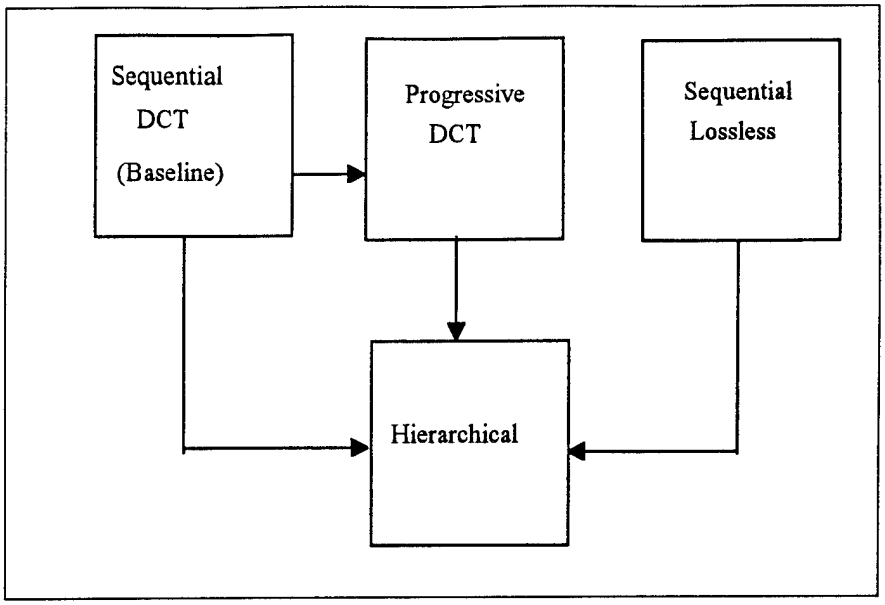

Figure 3.1 The four JPEG modes of operation (Pennebaker and Mitchell p.82)

1. Baseline JPEG

Baseline JPEG is the most common implementation of the JPEG standard. The JPEG standard refers to this as Sequential DCT coding. The baseline JPEG algorithm consists of the following steps:

a. Partitioning/Discrete Cosine Transform

The input image is first divided into 8 x 8 blocks of pixels. Each of these 8 x 8 blocks is then transformed using a two-dimensional forward Discrete Cosine Transform (DCT). The forward DCT used in the JPEG standard is defined as:

(13) $$F(u,v) = \frac{C(u)C(v)}{4} \sum_{j=0}^{7} \sum_{k=0}^{7} f(j,k) \cos\frac{(2j+1)u\pi}{16} \cos\frac{(2k+1)v\pi}{16}$$

$C(u), C(v) = \frac{1}{\sqrt{2}}$ for $u,v = 0$;

$C(u), C(v) = 1$ for $u,v \neq 0$ (Pennebaker and Mitchell p. 376)

As a result of this transformation, the average pixel value of the block is located as the upper left coefficient of the block. This is referred to as the DC term. The information contained in the other 63 coefficients, termed the AC coefficients, define the

higher frequency components of the block. After the DCT, the majority of these coefficients are zero or nearly zero and will be quantized to zero in the next step.

b. Normalization/Quantization

The next step in the baseline JPEG algorithm entails the normalization and quantization (as discussed in Chapter II) of each of the 64 coefficients. This is accomplished by applying a normalization array to the coefficients in the following manner (Rabbani, p. 177):

(14) $$F^*(u,v) = \text{Nearest integer } \frac{F(u,v)}{Q(u,v)} \approx \left\lfloor \frac{F(u,v)+\left\lfloor \frac{Q(u,v)}{2} \right\rfloor}{Q(u,v)} \right\rfloor$$

At this point, the 8 x 8 block is ready for coding. However, the coefficients are not coded in a row by row fashion. Since the bulk of the information about the block is contained in the upper left corner of the block, the coefficients are recorded using a zig-zag pattern (ordered from 0 to 63) as shown in Figure 3.2.

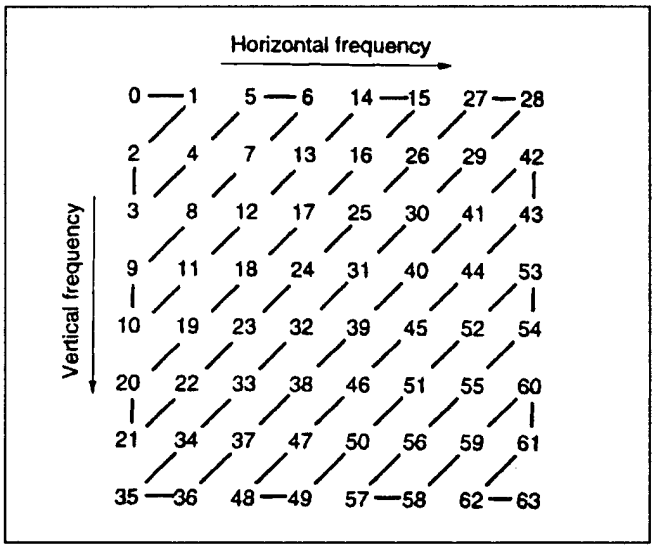

Figure 3.2 Zig-Zag Encoding Sequence (Pennebaker and Mitchell p. 172)

This pattern was chosen since the probability of the coefficients being zero is an increasing function of the index (Figure 3.3).

The zig-zag pattern thus maximizes the runs of zero coefficients which in turn simplifies the coding process.

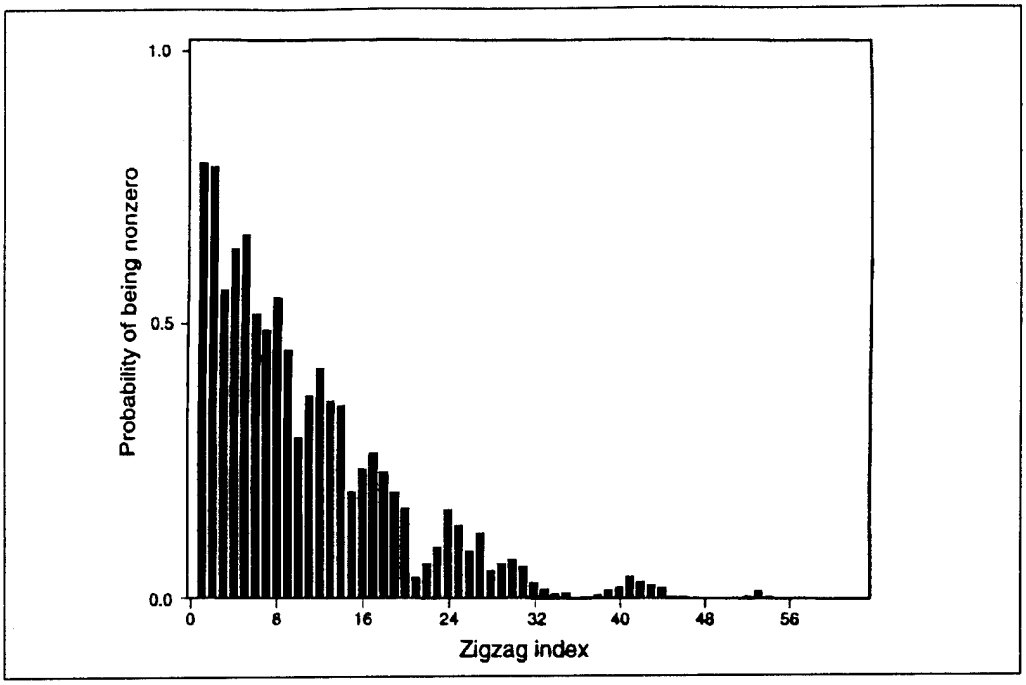

Figure 3.3 Probability of AC coefficient being zero (Pennebaker and Mitchell, p. 173)

c. DC Coefficient – DPCM Coded

The DC coefficient is then coded using Differential Pulse Code Modulation (DPCM). The process of DPCM coding is as described in Chapter II. The reason for this is first, the DC coefficient is a weighted average of the 64 pixels and as such is a good representation of the block as a whole. Additionally, there is generally a strong correlation between this coefficient and the DC coefficient of adjacent blocks, therefore DPCM coupled with a fixed Huffman encoding is particularly efficient.

d. AC Coefficients – Huffman Coded

The other 63 coefficients are encoded using a version of Huffman coding as shown in Rabbani, Pennebaker and Mitchell, Wallace and the ISO standard. First, each non-zero coefficient is expressed in an eight bit representation I=(NNNNSSSS) where the 4 most significant bits (NNNN) represent the number of zero coefficients between it and the last non-zero coefficient. Run lengths of more than 16 zeroes are coded using more than 1 symbol.

For example if the coefficients were ordered in the following manner, 79 0 -2 -1 -1 -1 0 0 -1 EOB; and the -2 coefficient was the one being encoded, the 4 most significant bits would be 0001 representing 1 zero between it and the previous non-zero coefficient (being the 79).

The 4 least significant bits (SSSS) define in which category the amplitude of the coefficient falls. The category (k) being defined as: $k=\lfloor \log_2(|\text{coefficient}|) \rfloor + 1$. Where $1 \leq k \leq 10$ for baseline JPEG.

Using the coefficient (-2) from before, k=2. Therefore the coefficient would be encoded as I = '00010010_2' .

I='11110000_2' represents a runlength of 16 zeroes and I=0 represents the end of block. The end of block signifies that all remaining coefficients in the block are zero. (Rabbani, p. 115)

These symbols (the 8-bit I's that represent the data stream) are Huffman coded using standard look-up tables These fixed tables are optimized to a particular probability distribution. If the image does not closely match this distribution, it is possible that the coding will actually cause image expansion vice compression. Again using the tables from Rabbani, the -2 coefficient is Huffman coded as '111001_2'.

Each Huffman character is appended by a sign bit (0 representing a negative coefficient) and an additional k-1 bits representing the magnitude of the coefficient within category k. So the final character transmitted to represent the -2 coefficient would be '11100101_2' . Once the entire image is encoded, it can be transmitted using standard digital transmission techniques. (Rabbani, p. 120)

e. Image Reconstruction

Upon reception of the compressed image, the reconstruction of the image follows the inverse process to the compression stage. The stream is first Huffman decoded using the same standard tables that were used to encode the data stream. The stream is then placed back into its 8 x 8 pixel representation and multiplied by the normalization/ quantization matrix. The inverse DCT is then applied to the matrix resulting in an approximation to the original image block.

(15) $f(j,k) = \frac{1}{4}\sum_{u=0}^{7}\sum_{v=0}^{7} C(u)C(v)F(u,v)\cos\left(\frac{(2j+1)u\pi}{16}\right)\cos\left(\frac{(2k+1)v\pi}{16}\right)$

$C(u), C(v) = \frac{1}{\sqrt{2}}$ for u,v = 0;

C(u), C(v) = 1 otherwise (Pennebaker and Mitchell p. 376)

2. Lossless JPEG

Inherent in using a quantizing step with the DCT is some introduction of error to the compressed and subsequently restored image. As there is a requirement in some circumstances (e.g., medical imagery, as documented by DICOM 3, and scientific imagery) for the exact image to be restored, ISO-JPEG established a lossless algorithm for those applications. Additionally, as the NITF standard is the government standard for the format of digital imagery and imagery products, the standard also establishes a lossless JPEG standard (MIL-STD 188-198A). To make the algorithm generic and not restrictive to the encoder and decoder design, a predictive coding method was chosen for the lossless implementation of JPEG. Figure 3.4 shows the main steps in producing a losslessly encoded image.

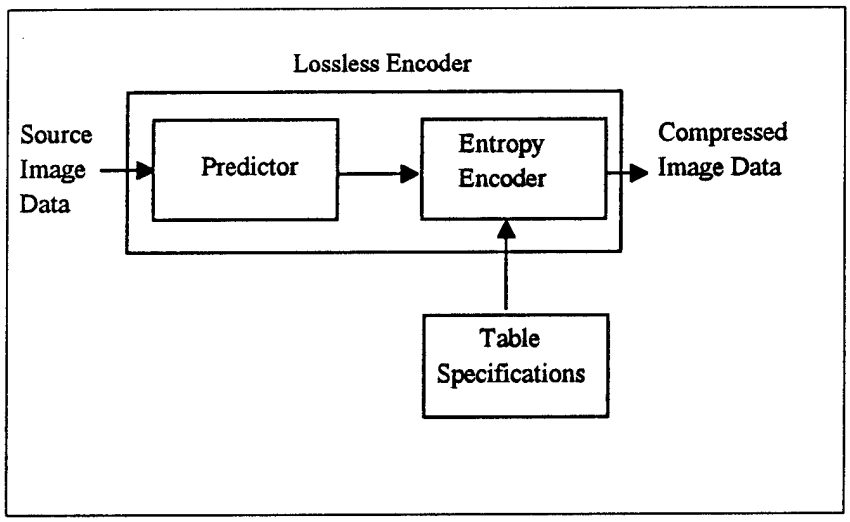

Figure 3.4 Lossless Mode Encoder Processing Steps (Wallace, p.7)

As discussed in Chapter II, the first step in compressing an image is transforming the pixel information. In the Lossless JPEG algorithm, this step is performed by predicting the pixel value based on the values of the neighboring pixel values (similar to DPCM). The Lossless algorithm is only concerned with the pixels shown in Figure 3.5 (x being the pixel

to be predicted and a, b and c being the neighboring pixels). This is because only pixels that have been previously coded may be used as predictors since their values are available to both the encoder and decoder. (Pennebaker and Mitchell p. 182)

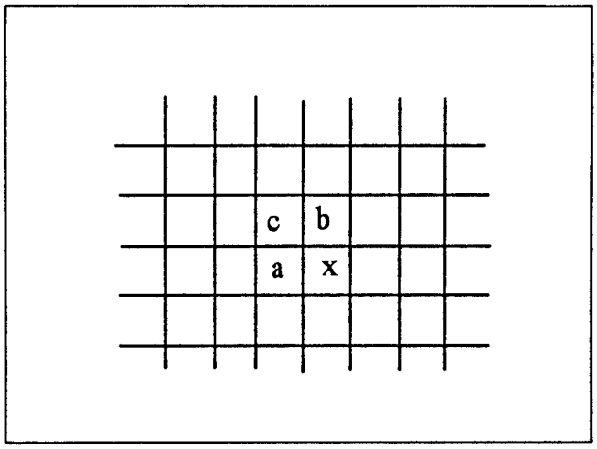

Figure 3.5 Relationship between pixel and the predictor pixels (Pennebaker and Mitchell p.184)

Table 3.1 shows the prediction equations used by the Lossless JPEG algorithm. Selection value 0 is used only for the hierarchical mode lossless coding. Selection 1 is used as a predictor for the first row of pixels. The first pixel in each subsequent row is predicted using selection 2. One of the remaining predictors is used to predict the remaining pixels. The predictor chosen is sent in the scan header of the image.

Selection Value	Prediction
0	no prediction
1	a
2	b
3	c
4	a+b-c
5	a+((b-c)/2)
6	b+((a-c)/2)
7	(a+b)/2

Table 3.1 Predictors for lossless coding (Pennebaker and Mitchell p. 492)

Once the prediction value is determined, the difference between the predictor and the original pixel value is computed. This difference is then losslessly entropy-coded using either Huffman coding or arithmetic Q-coding as described in Chapter II. Since there is

no quantization step involved in this process, and the coding step is lossless, the algorithm is then lossless.

In the decoder, the data stream is first entropy-decoded using the same Huffman or arithmetic coding technique. The difference is then added to the prediction to determine the original pixel value. Compression ratios of 2:1 are generally associated with the Lossless JPEG compression algorithm. (Pennebaker and Mitchell p. 78)

3. Progressive JPEG

The progressive mode of JPEG uses the same Forward Discrete Cosine Transformation and Quantization as in the baseline algorithm. The difference is that the coefficients are encoded in multiple scans rather than a single pass as in baseline JPEG. The first scan produces a rough version of the original. Each subsequent scan adds additional quality to the received image. The benefit to this is that each scan takes a relatively short time to transmit compared to the total transmission time. Additionally, some information that can be extracted rapidly is readily available to the tactical commander, rather than requiring an entire image to be transmitted before any evaluation can occur. There are two methods of progressive coding, spectral selection and successive approximation (Figure 3.6).

a. Spectral Selection

Spectral selection uses scans where only one particular frequency band is encoded at a time. The DCT coefficients are grouped into "spectral" bands of related frequency and then transmitted.. The lower frequency bands are typically transmitted first since this provides most of the rough detail of the image. The higher frequency components provide the fine line and texture detail in the image.

b. Successive Approximation

Successive approximation is a process where the coefficients are not encoded to their full accuracy in one pass. During the first pass a specified number of the most significant bits are encoded and transmitted. On subsequent passes the remaining bits are encoded and transmitted.

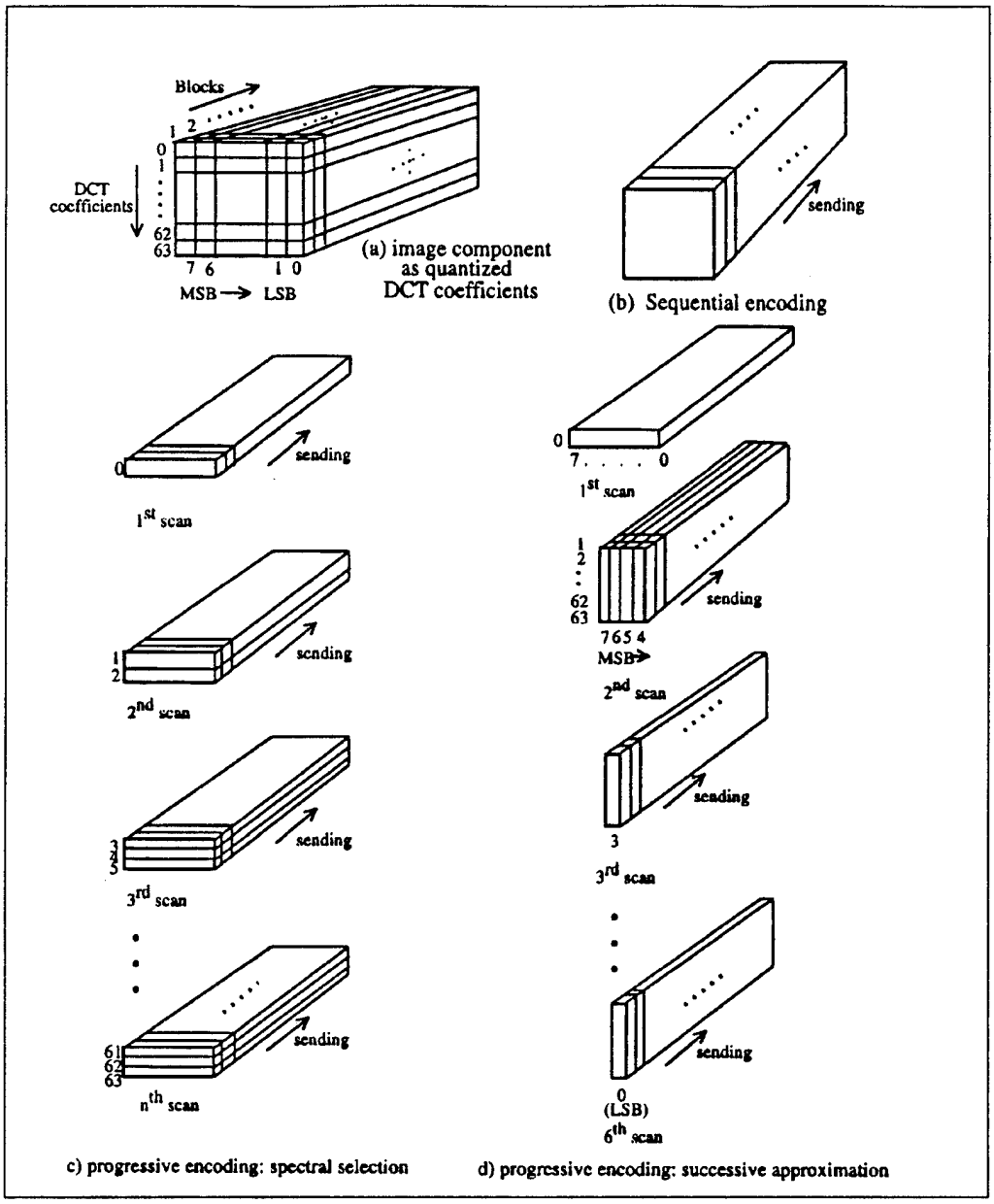

Figure 3.6 Progressive Encoding Models (Wallace, p. 14)

4. Hierarchical JPEG

The hierarchical JPEG mode encodes the image data so that images of various resolution levels can be restored on command. This provides the user with several options. The tactical commander can browse lower resolution imagery and then request those images of higher resolution, that he feels are useful. Additionally, the tactical commander can browse imagery, increasing the resolution only to the point where he can

exploit the information he requires. These approaches are a form of progressive coding. The other option is that the image can be supported by a variety of output devices (e.g., a high-quality printer ranging in resolution from 72 to 1200 dpi and a low-resolution video screen with 72 dpi resolution).

The method of hierarchical JPEG coding is rather simple and can be summarized by the following steps:

1. The original image is filtered and down-sampled by the desired number of multiples of 2 in each dimension.
2. The reduced-size image is encoded using one of the three previously discussed JPEG coding modes.
3. The reduced size image is decoded and then interpolated and up-sampled by 2 horizontally and/or vertically, using the identical interpolation filter that must be used by the receiver.
4. Use the up-sampled image as a prediction of the original at this resolution, and encode the difference image again using one of the three previously discussed JPEG coding modes.
5. Steps 3 and 4 are repeated until the full resolution of the image has been encoded.

Note that the encoding in steps 2 and 4 must be of the same type. (e.g., only DCT processes or only lossless processes). This process is shown in Figure 3.7. (Wallace, p. 13)

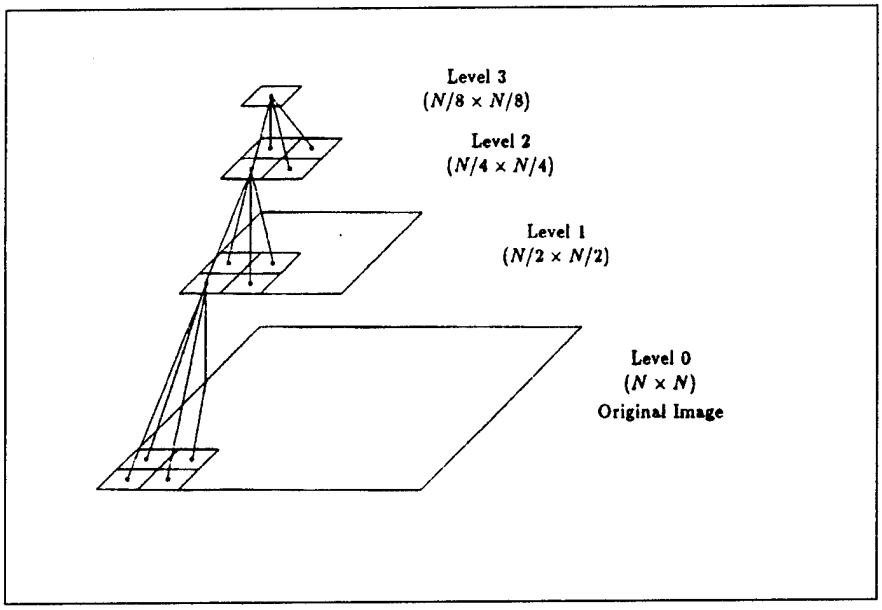

Figure 3.7 Hierarchical Compression Pyramid Structure (Rabbani, p 193)

5. Error Sources

There are several sources of error using the lossy implementations of JPEG. The obvious first source would be the Discrete Cosine Transform. As most hardware implementations use fixed precision, the use of the cosine function in the DCT will introduce small errors into the transformed coefficients. These are particularly noticeable on the inverse DCT since the input coefficients into the inverse DCT have been additionally quantized on encoding.

The second and probably the largest source of error is a result of the normalization/ quantization step. The error in the quantization step is discussed in Chapter II. The error introduced in the normalization step results from the use of the floor function. Any precision maintained by the division step is removed by using this function. Errors resulting from this step can be minimized by fine-tuning the normalization matrix used, however, complete elimination of the error is not possible.

Finally, error can be introduced as a result of the transmission process. Lost and/or modified bits can turn up in the received signal thus degrading the reconstructed image. These errors are unavoidable and again can only be minimized by fine-tuning the particular transmission process used or by using error detection and correction then retransmitting as required.

B. WAVELETS

1. Wavelet Application of Subband Coding

Wavelet compression is one type of subband coding. Wavelet compression implements the two-dimensional, four-band analysis bank in the form of Quadrature Mirror Filters (QMFs). The QMFs allow for alias-free reconstruction in the absence of coding errors. Additionally, the QMFs are designed to minimize overall amplitude and phase distortion of the signal. (Rabbani, p. 170)

2. Quantization

The quantization step employs either staircase or vector quantization. These quantization techniques are described in Chapter II.

3. Encoding

Once the wavelet coefficients have been quantized, they can then be coded by a variety of methods. These range from the simplest, run-length coding, to one of the newest forms of coding, zerotrees.

a. General Coding Methods

Run-length coding of the zero coefficients is one of the simplest coding methods. This method takes a run of zeros and encodes the length of the run using either a fixed codeword or using entropy coding. Generally, the remaining coefficients are not coded as they typically do not exhibit any type of run structure.

Additionally, entropy coding methods (such as Huffman or arithmetic coding) as discussed in Chapter II may be employed.

b. Zerotree Coding

Zerotree coding is a method developed by Jerome Shapiro of the David Sarnoff Research Center. Shapiro describes the zerotree coding algorithm in detail. Essentially a hierarchical relationship (parents to descendants) of wavelet coefficients is established. The subbands are arranged sequentially using a zig-zag pattern similar to that used in JPEG. Coefficients are then encoded using the process in Figure 3.8 where a coefficient, x, is insignificant with respect to a given threshold T if $|x| < T$.

4. Reconstruction of the Compressed Image

Reconstruction of the compressed image follows the inverse process. The received data stream is first decoded using the inverse coding process. The output stream is then put through a two-dimensional, four-band synthesis bank (Figure 3.9) where the reconstructed image is the output.

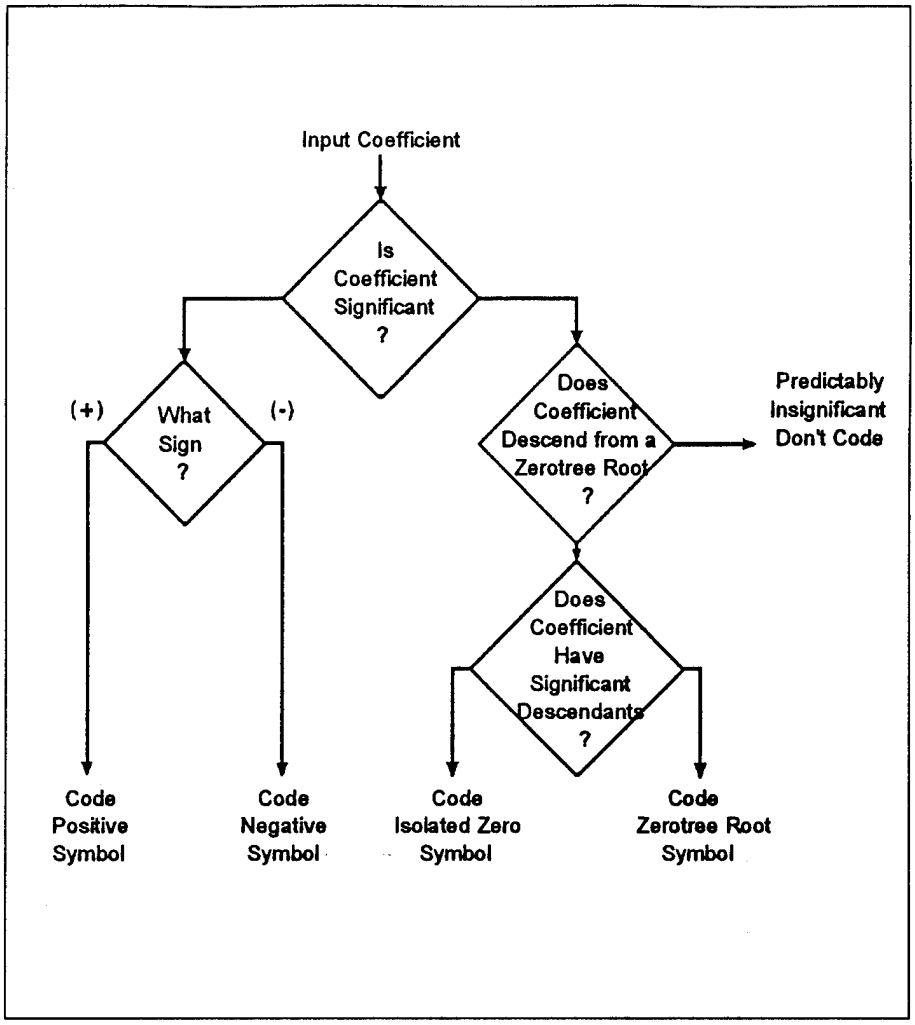

Figure 3.8 Flow chart for encoding a coefficient of the significance map (Shapiro, p. 3450)

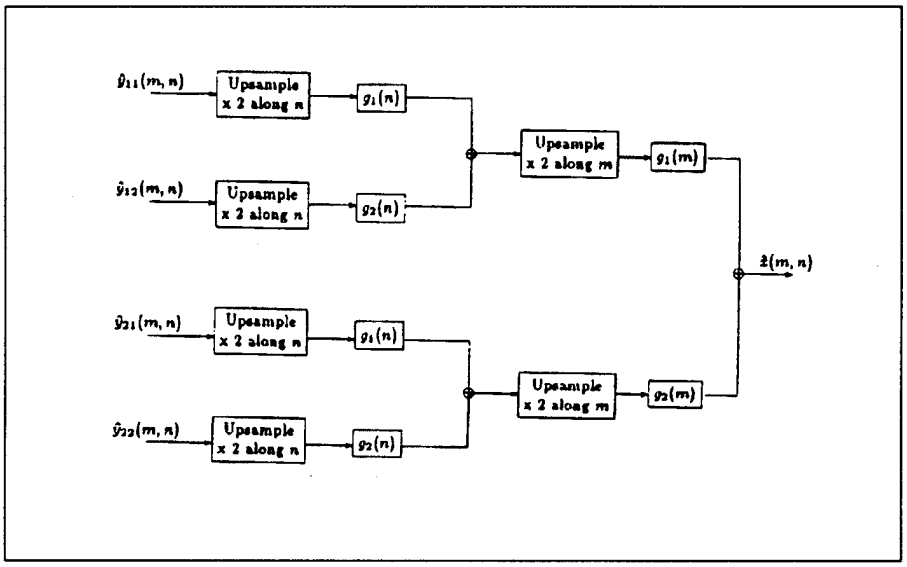

Figure 3.9 2-D, four-band synthesis bank (Rabbani, p. 175)

5. Error Sources and Effects

Using Wavelet compression, there are several places in the algorithm where error can be introduced. First would be in the subband coding process. Certain subbands that do not meet a specified threshold can be discarded prior to the quantization stage. This will obviously introduce errors since those subbands will not be present for the reconstruction step. Additionally, the use of Quadrature Mirror Filters (QMF) introduces some error into the signal. Inherent in the QMF is some amplitude distortion. Larger filters will reduce the distortion but will however increase the computational load (Rabbani, p. 173). Therefore tradeoffs must be made between acceptable error introduced by the QMFs and the additional computational load resulting from the larger filter.

Second would be the quantizing step itself. The use of a standard staircase function quantizer will force some of the smallest coefficients to zero and will reduce the precision of others. The choice of the particular quantizer function is critical however. If the steps are too large, an enormous amount of error can be introduced into the data stream. On the other hand, if the steps are too small, the data stream may actually become larger than the input data set.

Using the zero-tree coding method another source of error is introduced. Again, by assigning a threshold which makes certain coefficients "insignificant," if their magnitude is below that level, this will also remove some information from the data stream.

Finally, just as in JPEG and the other compression algorithms, the transmission process can introduce some error. While none of the above errors can be eliminated, fine-tuning in each of the steps can reduce the errors to a large extent.

C. FRACTAL COMPRESSION

1. How are Fractals Applicable to Image Compression?

Fractal image compression has been likened to a specially designed copying machine. The classic illustration is shown as a copy machine which will take an input image, reduce the image in half and then output the image in a particular array on the copy. An example of this is shown in Figure 3.10. (Fisher, p. 2)

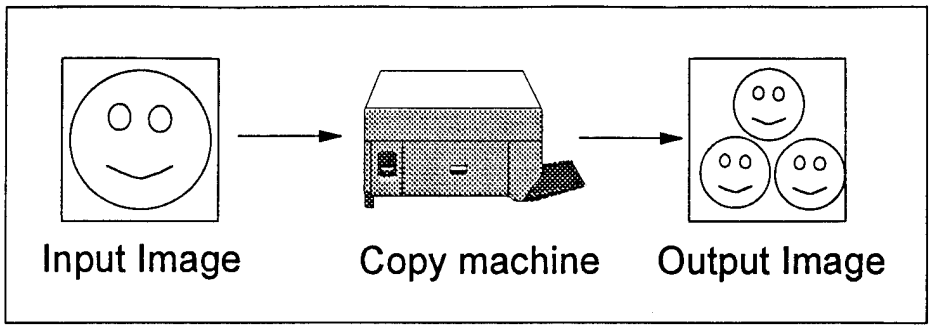

Figure 3.10 Copier Analogy (Fisher, p. 3)

Using this particular copying machine, if the output is then looped into the copier as the next input image, the output will eventually converge on an image called the Sierpinski triangle, Figure 3.11.

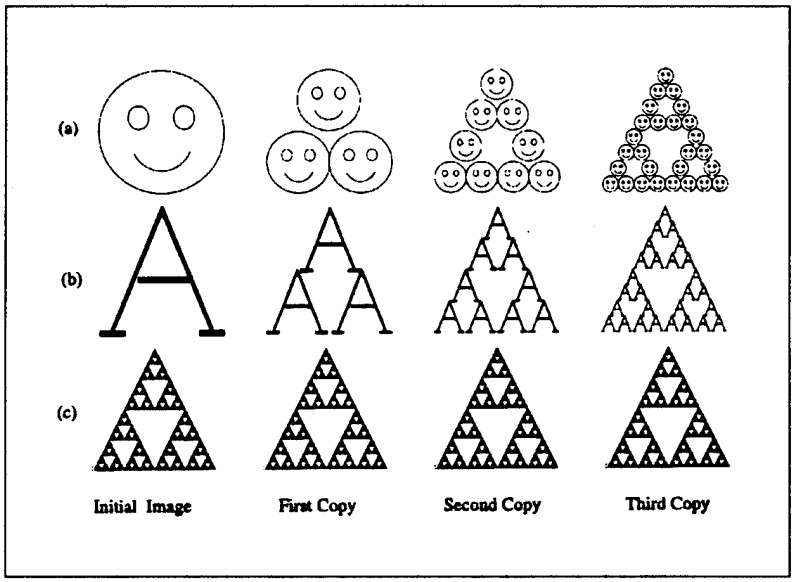

Figure 3.11 First three copies using copier in Figure 3.10 (Fisher, p. 4)

What makes this particular copying machine unique is that any initial input image can be used and will result in the Sierpinski triangle. The Sierpinski triangle is termed the attractor for this machine. The goal of fractal compression is to determine the transformations required (the copying machine) in order to obtain the appropriate output image.

In practice, affine transformations expressed as:

$$(16) \quad w_i\begin{bmatrix} x \\ y \end{bmatrix} = \begin{bmatrix} a_i & b_i \\ c_i & d_i \end{bmatrix}\begin{bmatrix} x \\ y \end{bmatrix} + \begin{bmatrix} e_i \\ f_i \end{bmatrix}$$

are used. These transformations can skew, stretch, rotate, scale and translate the input image (Fisher, p. 3).

The use of this particular copy machine, however, requires that the desired output image be made up of copies of itself that have been transformed using the above affine transformations. This is to say the image has detail at every scale. This is the classical definition of a fractal image. (Fisher, p.3)

Unfortunately, while many naturally occurring objects may be represented by fractal images, there are a considerably larger number that cannot. While the images that the tactical commander requires generally are not fractal images, there are portions of the image that can be represented by larger portions of the image. Fractal compression is therefore designed to reduce this redundancy and allow it to be represented using these affine transformations.

Fractal compression, in general, is a relatively simple process. First the image is partitioned into a number of groups of pixels termed ranges (R_i). For each range, a larger piece of the image, a domain (D_i), is sought that best approximates the range within a given tolerance error (Figure 3.12). The range may be represented by any orientation of a domain. While fixed size ranges and domains may be easily implemented, typically different variations of this approach are chosen. These partitioning schemes are described in the following Sections.

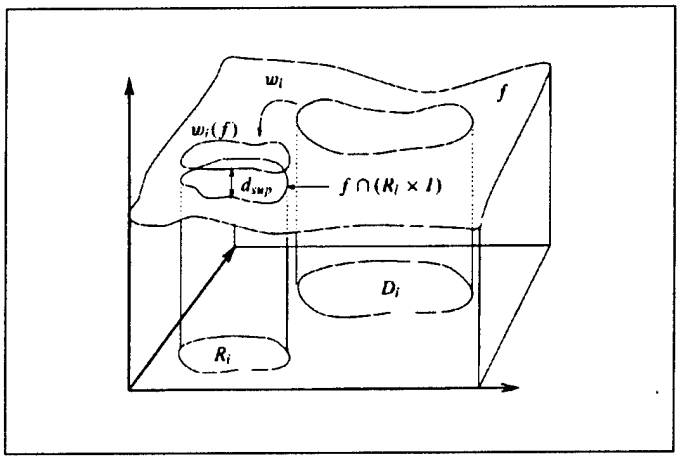

Figure 3.12 Relationship between Domain and Range (Fisher, p. 12)

2. Fractal Compression using Quadtree Partitioning

Quadtree partitioning is an approach to fractal compression where the ranges and domains are of variable sizes. This is useful in that areas of detail in the image can be represented by smaller ranges whereas large non-detailed regions (large expanses of cloudless sky for example) can be represented by larger ranges.

In determining the ranges, the image is first taken as a whole. As it is generally not well represented by a range that covers its entire dimension, the image is divided into 4 equal partitions. Each of these partitions is then examined to see if it can be represented by a domain within the established tolerance level. Each domain is twice the size of the range. The pixels in the domain are averaged in groups of four, reducing the domain to the range size. The range is checked against all 8 possible orientations of the domain (90° rotations of the domain and of the mirror image of the domain). The transformation of the pixel values is found that will minimize the root mean square (rms) difference between the transformed domain and actual range pixel values. Any partition that cannot be depicted by a domain within the rms level is further subdivided into 4 partitions. This process then continues until the entire image is represented (Figure 3.13). The accumulation of these transforms is the encode (i.e., compression) of the image. (Fisher, p 16).

Unfortunately, the comparison of each range against all domains is time-consuming and computationally intensive. In order to reduce the number of computations and to reduce the period of time for encoding, all domains are classified before any ranges are created. Once this is done, each range is first classified and then only compared against domains with the same or similar classifications. This process significantly reduces the number of comparisons made, thereby reducing the number of computations and the amount of time required to compress the image.

Reconstruction of the compressed image is rather straight-forward. First, each domain that has been mapped to a range is reduced by averaging each 2x2 group of pixels. This reduces the domain by 2 in each dimension. The new domain pixel values are appropriately scaled and the associated offset value is applied. The domain is then placed, as applicable, into the range. This process is iterated until additional iterations do not change the reconstructed image or are below the given tolerance level. (Fisher, Ch 3)

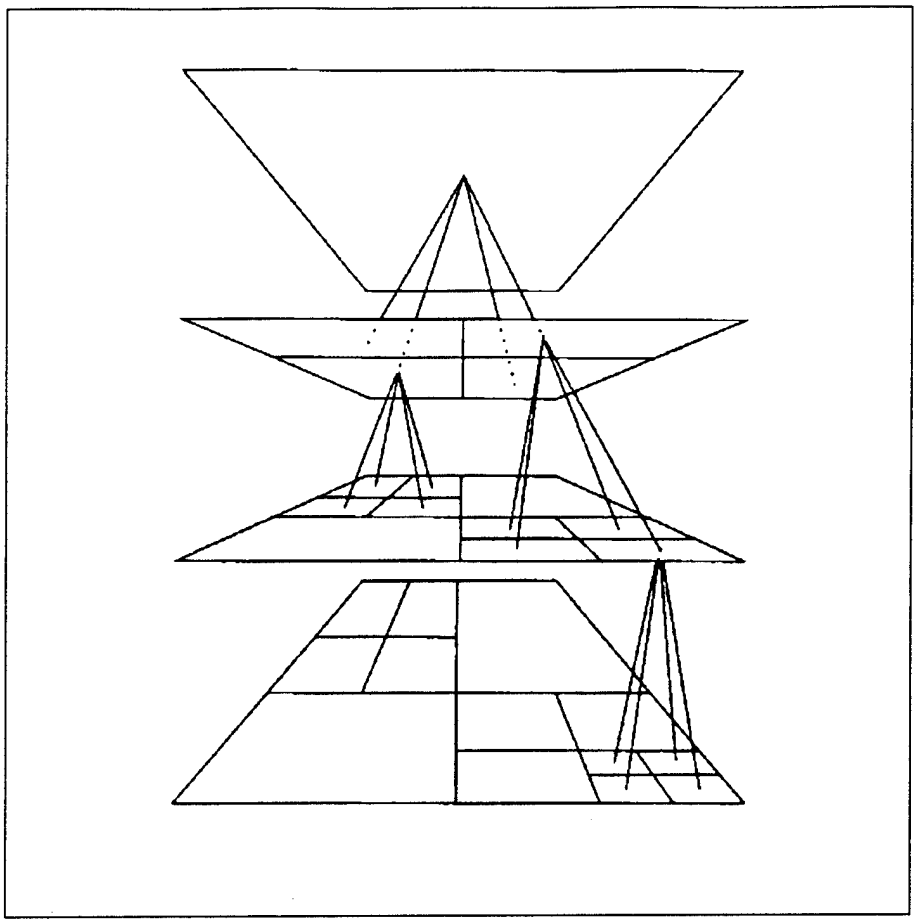

Figure 3.13 A quadtree representation of an image (Fisher, p. 56)

3. Fractal Compression using HV Partitioning

Fractal compression using HV partitioning uses a similar approach as that described for compression using quadtree partitioning. First, the image is partitioned into two rectangles. This is accomplished by determining the average pixel value for each row and column in the image. Successive differences are calculated between the averages. Applied to each of these differences is a linear biasing function. This consists of multiplying each difference by the distance from the nearest side of the image. The maximum magnitude of these results, either horizontally or vertically is where the partition is made.

Again, similar to the quadtree approach, the ranges are compared against the associated domains. Each domain is larger than the range it is compared against by either a factor of 2 or 3. This factor can differ on each side. The domain pixels are averaged

again in 2x2 blocks of pixels. The range is then represented by the domain giving the smallest square difference within the given threshold. If no domain can satisfy this constraint, the range is further partitioned using the same procedure as above. This process is repeated until the image ranges are all represented by domains satisfying the threshold or until the range size is smaller than the threshold.

There are several methods that Fisher mentions to speed up the algorithm. The first of these is similar to the classification process described in quadtree partitioning. Each domain and range is classified prior to search. Thus only domains that are in the same or similar classification as the range are compared. The second method is termed "encoding by range size." The largest range available is the first chosen for comparison. The largest range is determined by the range having the largest, smaller dimension (e.g., a 10x8 range will be compared against the domains prior to a 20x7 range.) This allows the ranges to be mapped in decreasing size order thereby eliminating the repetition of domain classifications.

Decompression of the image however utilizes a more efficient algorithm than that employed by the quadtree method. There are two processes that are responsible for the increased efficiency, Pixel Referencing and Low-dimensional Fixed-point approximation. Fisher describes these processes in detail in his book Fractal Image Compression.

D. RADIANT TIN

The Radiant Tin algorithm is an innovative way of approaching image compression. Typically, lossy image compression is achieved through 3 steps: transformation, quantization and coding. Instead of the typical transformation step however, the Radiant Tin algorithm takes the original image in its pixel space representation and converts it into a symbol space representation.

This conversion extracts features; such as edges, arcs, and textures, and then converts them to symbols, in vector space, representing these features. These symbolic representations consist of start point and end point information, texture information statistical information defining shape and color standard deviation, relational information and geometric information defining direction and length. (ISOA, p. 3)

The conversion process used by the Radiant Tin algorithm is a two step process. The first step is the determination of edges in the image. These edges are found using a modified Sobel filter. This Sobel filter kernel has been modified so as to maximize the ability to extract edge information. The Sobel filter is a type of gradient operator consisting of four 3x3 masks. These masks are convolved with the image. The resulting vector gives the magnitude of the gradient as well as its direction. Gradients exceeding a predetermined threshold are considered edges.

Once the starting point of the edge has been determined, the edge can proceed in only one of three directions: left, forward or right. Each edge is then traced pixel by pixel. The start point, the end point, the starting direction (this may be any of 8 directions), the length of the edge in pixels and the directional changes (0 for left, 1 for forward and a 2 for right) are recorded in tabular format. An example of this table is shown below:

Start Point		End Point		Start Dir	Edge Length	Directional Changes.
212	117	201	2	1	68	'20120202020112102020120120
75	194	115	22	1	216	'01120120120120210210210211
113	165	76	36	2	42	'12021021102102020112011111
137	49	252	38	3	125	'02111111021111102102110202

Table 3.2 Example Edge Data

The second step is concerned with the texture information on either side of the edge. The average textures on both the right and left sides of the line are determined and are recorded. These textures are used to provide the gradient information for the edge determination as well as for image reconstruction.

Once the edges have been determined, Radiant Tin provides two methods as options used to transform and code the image. The first uses the symbolic image. Only the areas of the image where symbols exist are transformed using a modified Mallat wavelet transform. The resulting coefficients are subtracted from the wavelet transform of the entire original image. This leaves only the texture information of the original image which is then coded using a different wavelet transform.

The second method performs transforms in the spatial domain using a residual error coding approach. The symbolic information from the edge determination is compressed and then restored. This information is then subtracted from the original image. The remaining data is then transformed using a modified wavelet transform. This method is diagrammed in Figure 3.14.

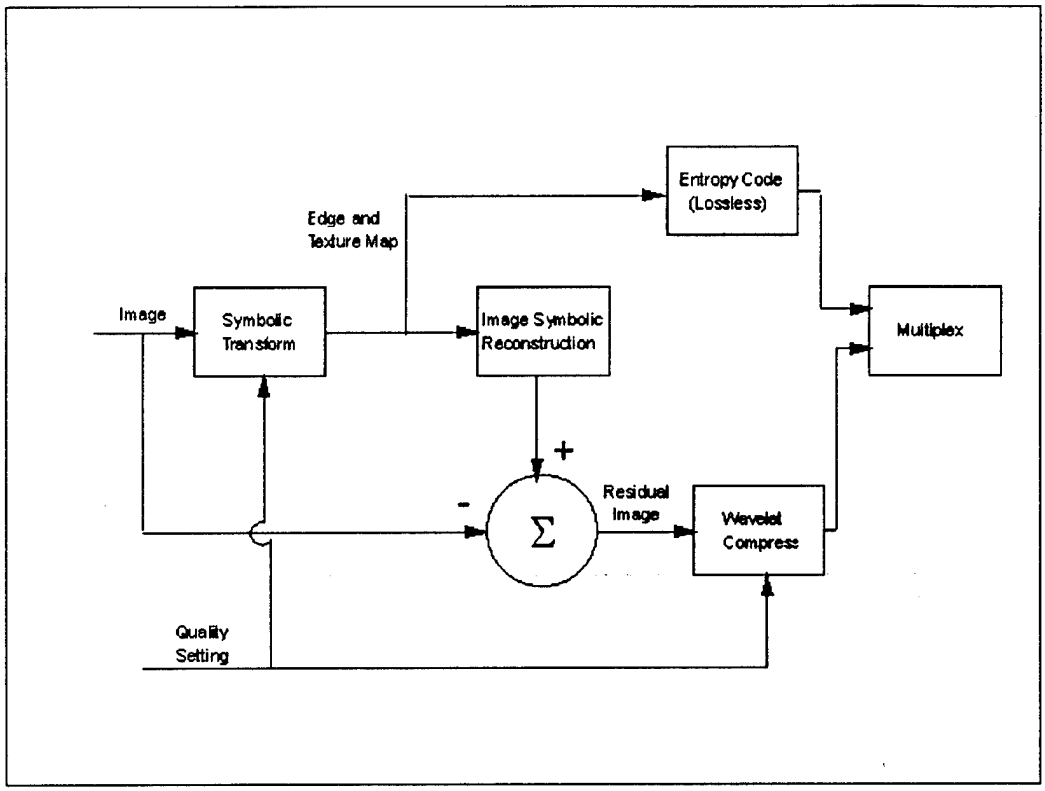

Figure 3.14 Radiant-Tin Spatial Transformation Flow Diagram (Beser)

Various levels of compression are achieved by modifying the quality setting (Q - a value of 1 to 100) upon calling the compression routine. The Q-value determines the amount of texture information (first method) or residual data (second method) that is coded. The higher the Q-value the larger the compression ratio. Additionally the Q-value is used to select the amount of segment data that is detected by the edge algorithm.

The Radiant Tin compression algorithm, using either symbolic decomposition or frequency decomposition, is shown in Figure 3.15.

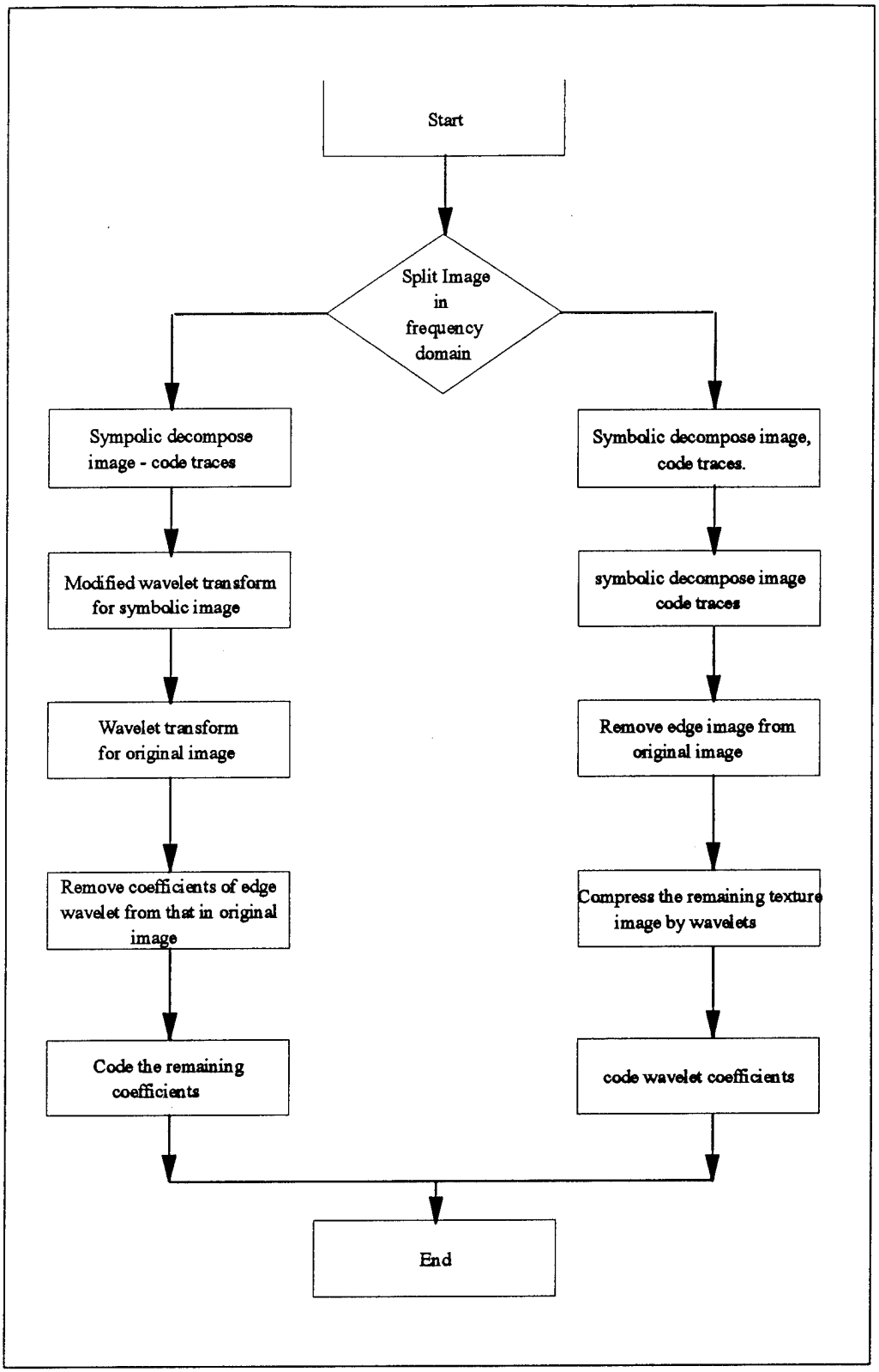

Figure 3.15 Radiant Tin Compression Algorithm (ISOA, p. 23)

IV. IMAGERY

A. COLLECTION SYSTEMS/SENSORS

1. Passive Visible-Near Infrared Sensors

a. Photographic Systems (Framing Cameras)

A framing camera collects imagery just as its name implies; it takes a "snapshot" of the particular area in view. The camera optics then project this "snapshot" on film, return beam vidicon or a two-dimensional array of detectors in the camera focal plane (Elachi, p. 89). Film systems include the Tactical Airborne Reconnaissance Pod System (TARPS) used on the F-14 and the old Corona reconnaissance satellite system (Wilson, p. 183). Early Landsat satellites use the return beam vidicon which is similar to a television camera, while digital handheld cameras are the best example of systems using a detector array (Cracknell and Hayes, p. 29) .

Film framing cameras are particularly advantageous for their large image format, high information density and cartographic accuracy. A distinct disadvantage to film systems is in the transmission of the film and the potential for image smearing. The broad spectral range, digital format of the data and the ability to simultaneously sample the image are favorable attributes of the electronic framing camera. However, there is the drawback with the difficulty in getting large arrays or surfaces with sufficient sensitivity (Elachi, p. 99). A generic photographic system is shown in Figure 4.1.

b. Scanning Systems

Scanning Systems utilize a rotating scanning mirror which places the image resolution element on a single detector. To cover the entire scene, the mirror scans perpendicular to the ground track of the platform. Typically, several detectors are used to allow several "lines" of data to be obtained simultaneously. This system is shown in Figure 4.1. Examples of scanning systems include the Multispectral Scanner and the Thematic Mapper both employed on the Landsat satellite system.

Scanning systems have several advantages. First, they contain simple detectors coupled with narrow field-of-view optics. They also have wide sweep capability and are particularly easy to use with multiple wavelengths. They are not without their disadvantages, the most important of which is moving parts. Additionally, there is a low detector dwell time which is associated with the difficulty in obtaining good geometric fidelity in the image. (Elachi, p. 99)

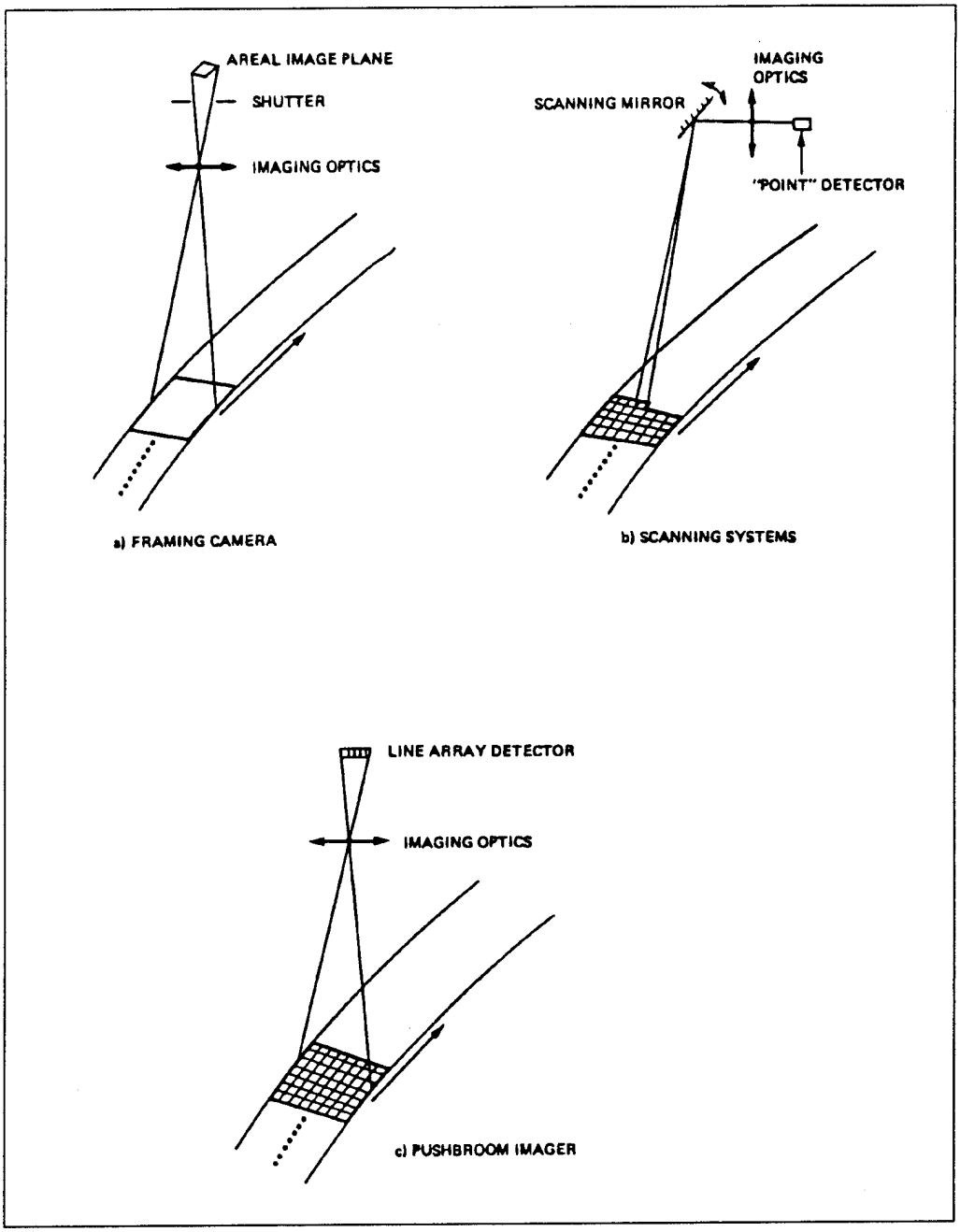

Figure 4.1 Different Imaging Systems (Elachi, p. 98)

c. Pushbroom Systems

Pushbroom systems use a linear array of detectors rather than the scanning mirror employed by scanning systems. As such, the entire cross-track area is covered simultaneously. Similar to scanning systems, the down-track motion of the platform results in the imaging of the scene of interest. The apparent "motion" down-track of the line of detectors is what gives the pushbroom system its name. This system is also depicted in Figure 4.1. The SPOT camera is an example of a pushbroom system.

What gives the pushbroom system the advantage over a scanning system is that it permits a much longer dwell time on each surface element which provides greater sensitivity as well as across track geometric fidelity. The wide field of view of the optics however, is a disadvantage.

2. Thermal Infrared Sensors

Thermal Infrared Sensors generally use a scanning approach to imaging. The development in the 1960s of the electro-optical linescanner, allowed for the recording of thermal energy. Thermal emissions are sensed, passively, by the detectors and converted to light energy which is recorded on film. An infrared scanning system can be seen in Figure 4.2.

Presently, thermal detectors are not as sensitive as visible and near-infrared detectors. In addition, thermal emissions are not as strong as those in the visible and near-infrared region. This results in thermal sensors with lower resolution and longer dwell times than the visible and near-infrared sensors. This corresponds to an increase in thermal noise which is counteracted by cooling the thermal sensors.

3. Active Microwave

a. Synthetic Aperture Radar

A Synthetic Aperture Radar (SAR) overcomes the inability to mount a radar antenna of sufficient size on a spacecraft. The SAR uses the consecutive positions of the antenna as it moves along track to recover the reflected signal. The motion along track

simulates an antenna varying from hundreds of meters to a few kilometers in length (Cracknell and Hayes, p. 42).

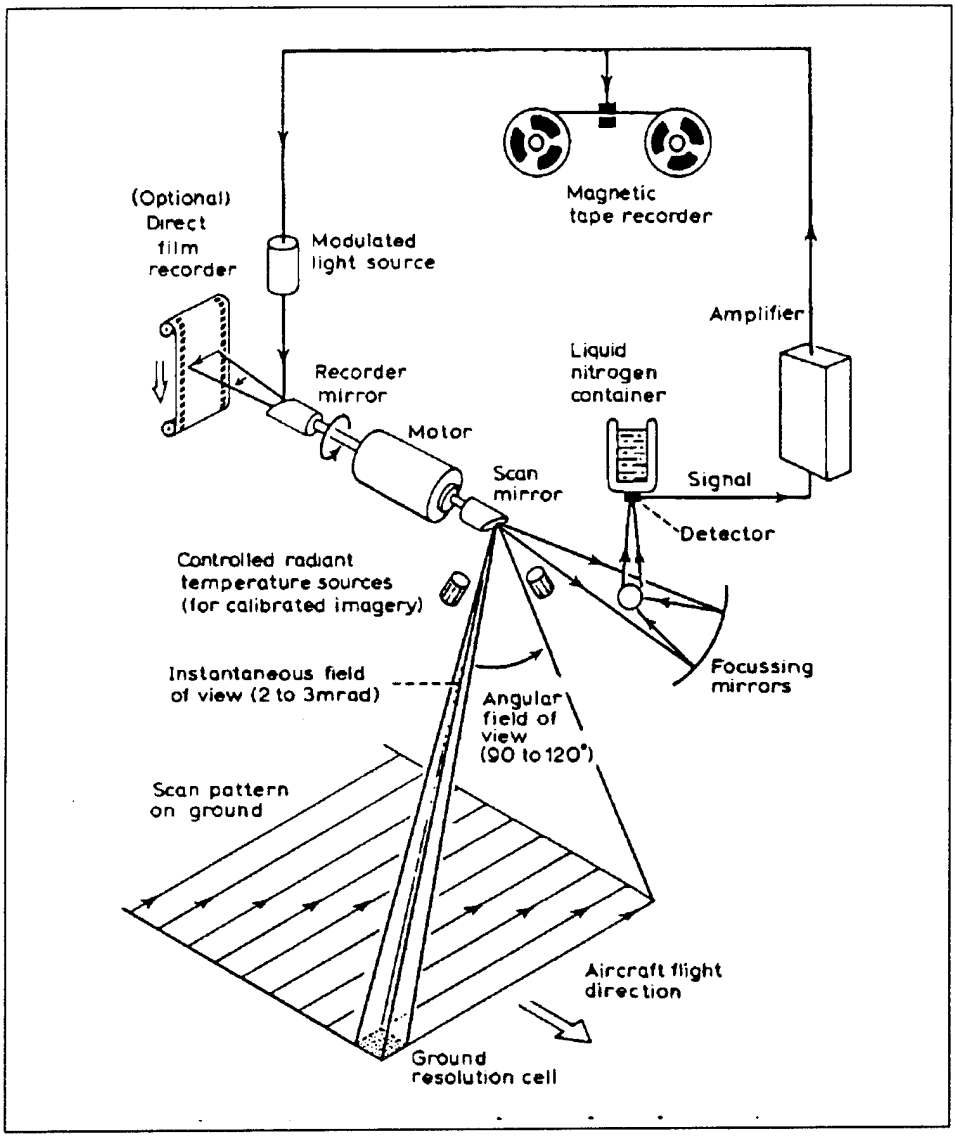

Figure 4.2 Thermal Imaging System (Cracknell and Hayes, p. 34)

There is an inherent disadvantage to the SAR system in that it requires significant computing power to correlate the Doppler phase history, which is used to generate the SAR image. This processing does include some problems in that the algorithm cannot distinguish between Doppler shifts resulting from the motion of the platform and the motion of objects sensed (e.g., moving trains, ships, etc.). As such, the Doppler shifts are additive and may result in object displacement (i.e., a train from its tracks or a ship from its wake).

B. COLLECTION PLATFORMS

The discussion here of collection platforms is not meant to be an exhaustive list of platforms capable of collecting imagery. It is provided to demonstrate the wide variety of platforms as well as provide the reader with an appreciation for the limitless uses for imagery products.

1. Satellites

a. Landsat

Landsat is a NASA/DoD integrated system, designed to provide multispectral land, surface and ocean data. It's original mission was to "demonstrate the feasibility of multispectral remote sensing from space for practical Earth resources management practical applications" (Muolo, p. 86). Two of the largest applications of Landsat data are mapping land cover and monitoring aquatic and terrestrial change. Combinations of the multispectral imagery with visible and infrared images can be used to detect man-made objects that have been camouflaged to blend with the background (Muolo, p. 144). The current system can cover the earth (minus the poles) in 16 days and relay data in near real time using the Tracking and Data Relay Satellite System (TDRSS). (Muolo, p. 86)

b. SPOT

The Système Pour l'Observation de la Terre (SPOT) is a French satellite system designed by the Centre National d'Études Spatiales (CNES - the French Space Agency) for Earth observation and subsequent distribution of the images it collects. During the Gulf War, the SPOT satellites were used to provide multispectral imagery that was used for tactical planning, map updates and terrain analysis since they provide finer resolution than the Landsat satellites (Muolo, p. 144). The SPOT satellites are in a 97.8° inclination, 500 nm sun-synchronous orbit with a repeat interval of 26 days.

c. DMSP

The Defense Meteorological Satellite Program (DMSP) is a joint-use (military and civilian) program. The DMSP satellites are designed to generate weather data for the

U.S. operational forces worldwide. Additionally, through the National Oceanographic and Atmospheric Administration, the meteorological data is furnished to civilian users. The satellites provide real time weather information to aid the commander in mission decision making. The information is "invaluable in supporting the launch, en route, target and recovery portions of a wide variety of strategic and tactical missions." (Muolo, p. 94) The satellite is in a Low-Earth orbit of 450 nm. It is in a near-polar, sun-synchronous orbit allowing for total Earth coverage in approximately 12 hours. The satellite has a ground track width of 1,600 nm.

2. Reconnaissance Aircraft

Before World War I, reconnaissance was the only role imagined for aircraft during time of war (Gunston, p. 7). While this quickly was disproved, the reconnaissance mission is still a high priority. Aircraft are probably the tactical commander's most rapid response to an imagery requirement. The biggest disadvantage to using reconnaissance aircraft for collecting imagery is that, with today's weaponry, the aircraft are ordinarily well within the air defense envelope of the adversary. So while this may make space-based collectors more attractive, one still must consider the advantage of higher resolution imagery from these platforms.

Some examples of reconnaissance aircraft include:

- SR-71
- U-2/TR-1
- OV-1 Mohawk
- RF-4 Phantom
- TARPS equipped F-14 Tomcat
- Unmanned Aerial Vehicles

3. Others

Other platforms include ships, submarines and land-based tactical units, such as Navy SEALS, Marine Reconnaissance Units, and Army Special Forces. The sensors employed by these platforms include digital as well as film-based hand-held cameras.

Additionally, ships and submarines may be outfitted with specially designed electro-optical sights from which imagery may be obtained.

C. THE TACTICAL NATURE AND USE OF IMAGERY

Tactical reconnaissance has been defined as "that reconnaissance which provides information to the tactical commander (ground and air) for his use in the preparation for and implementation of tactical warfare" (Reamer, p. 4). In the past, this definition generally applied to a select group of imagery that was archived or obtained by tactical assets (i.e., aircraft) available to the tactical commander. With the increased emphasis on the "sensor to shooter" concept, the number of images that will become available to the tactical commander will only continue to grow and the definition of tactical imagery will only blur.

Imagery is important in all phases of Battlespace Management ranging from the initial Intelligence Preparation of the Battlefield, to the assessment of Battle Damage. Within the Intelligence Preparation of the Battlefield, imagery is used to assist in battlefield definition, situation assessment and threat analysis. This carries through to the Targeting phase where the emphasis is in determining the individual targets as well as a prioritization scheme. Once the targets have been determined, imagery is used during the Weaponeering phase to determine the best weapon to be used against the target as well as the selection of the weapon aimpoint. Finally, once the weapon has been placed against the target, imagery is used during the Battle Damage Assessment (BDA) phase for the determination of Combat Effectiveness against established Measures of Performance and Measures of Effectiveness. (Boger and Jones)

D. IMAGES SELECTED FOR THIS ANALYSIS

There were six images chosen for this analysis. They were selected for specific tactical information as well as their ability to test the strengths and weaknesses of the algorithms (such as edges in the image). The images were selected from a variety of TARPS and Hand-Held Digital Camera images held by the Johns Hopkins University Applied Physics Laboratory. The six images are shown in Appendix A with the specific points chosen for image comparison annotated on each.

V. MEASURES

A. QUANTITATIVE MEASURES

There are a variety of quantitative measures that have been used to judge the quality of reconstructed imagery. They generally fall into four categories: those based on an image model, those that are derived from signal processing, those based on a Human Visual System (HVS) model and graphical techniques. These measures are all bivariate (i.e., based on both the original and reconstructed image) and as such, measure the statistical difference between the two images. In each of the measures described in the following sections, F(j,k) is the original pixel value at position (j,k) in the image and $\hat{F}$(j,k) is the pixel value in the reconstructed image. The quantitative measures in Sub-Sections 1, 2 and 4 are those compiled by Eskicioglu, Fisher and Chen in their paper "Image Quality Measures and their Performance."

1. Techniques Based on an Image Model

a. Average Difference

$$(17) \quad AD = \sum_{j=1}^{M} \sum_{k=1}^{N} [F(j,k) - \hat{F}(j,k)]/MN$$

b. Maximum Difference

$$(18) \quad MD = Max\{\left|F(j,k) - \hat{F}(j,k)\right|\}$$

c. Laplacian Mean Square Error

The Laplacian Mean Square Error is used to demonstrate the correlation among adjacent pixels in the reconstructed image as compared to the original image. The idea here is that the strong correlation in these adjacent pixels will not be as strong in the reconstructed image.

$$(19) \quad LMSE = \sum_{j=1}^{M-1} \sum_{k=2}^{N-1} [O\{F(j,k)\} - O\{\hat{F}(j,k)\}]^2 / \sum_{j=1}^{M-1} \sum_{k=2}^{N-1} [O\{F(j,k)\}]^2 \text{ where}$$

(20) $O\{F(j,k)\} = F(j+1,k) + F(j-1,k) + F(j,k+1) + F(j,k-1) - 4F(j,k)$

d. Normalized Absolute Error

(21) $NAE = \sum_{j=1}^{M}\sum_{k=1}^{N} \left| O\{F(j,k)\} - O\{\hat{F}(j,k)\} \right| / \sum_{j=1}^{M}\sum_{k=1}^{N} |O\{F(j,k)\}|$

where the function O is defined in three ways:

(22) $a.\ O\{F(j,k)\} = F(j,k)$

(23) $b.\ O\{F(j,k)\} = F(j,k)^{\frac{1}{3}}$ and

(24) $c.\ O\{F(u,v)\} = H\{(u^2+v^2)^{\frac{1}{2}}\}F(u,v)$ in the cosine transform domain.

In equation 24, the function H is one that attempts to model the human visual system and is that function defined by Nill (Equation 29).

(25) $$H(r) = \left\{ \begin{array}{c} 0.05r^{0.554} \text{ for } r < 7 \\ e^{-9[|\log_{10} r - \log_{10} 9|]^{2.3}} \text{ for } r \geq 7 \end{array} \right\}$$

where $r=(u^2+v^2)^{0.5}$ and u, v are the coordinates in the transform domain.

These definitions for the function O are the same used in the Normalized Mean Square Error which is defined below.

e. L_p-Norm

(26) $L_p = \{\frac{1}{MN}\sum_{j=1}^{M}\sum_{k=1}^{N} \left| F(j,k) - \hat{F}(j,k) \right|^p\}^{\frac{1}{p}},\ p = 1,2,3$

2. Techniques Derived from Signal Processing

a. Structural Content

(27) $SC = \sum_{j=1}^{M}\sum_{k=1}^{N} [F(j,k)]^2 / \sum_{j=1}^{M}\sum_{k=1}^{N} [\hat{F}(j,k)]^2$

b. Normalized Cross Correlation

(28) $NK = \sum_{j=1}^{M}\sum_{k=1}^{N} F(j,k)\hat{F}(j,k) / \sum_{j=1}^{M}\sum_{k=1}^{N} [F(j,k)]^2$

c. Correlation Quality

$$(29) \quad CQ = \sum_{j=1}^{M}\sum_{k=1}^{N} F(j,k)\hat{F}(j,k) / \sum_{j=1}^{M}\sum_{k=1}^{N} F(j,k)$$

d. Image Fidelity

$$(30) \quad IF = 1 - \left(\sum_{j=1}^{M}\sum_{k=1}^{N} [F(j,k) - \hat{F}(j,k)]^2 / \sum_{j=1}^{M}\sum_{k=1}^{N} [F(j,k)]^2 \right)$$

e. Peak Mean Square Error

$$(31) \quad PMSE = \frac{1}{MN} \sum_{j=1}^{M}\sum_{k=1}^{N} [F(j,k) - \hat{F}(j,k)]^2 / [Max\{F(j,k)\}]^2$$

f. Normalized Mean Square Error

$$(32) \quad NMSE = \sum_{j=1}^{M}\sum_{k=1}^{N} [O\{F(j,k)\} - O\{\hat{F}(j,k)\}]^2 / \sum_{j=1}^{M}\sum_{k=1}^{N} [O\{F(j,k)\}]^2$$

where the O function is defined as in the Normalized Absolute Error measure.

3. Techniques Based on the Human Visual System

Quantitative measures, in general, do not correlate well with subjective quality measures. It is suspected the reason for such poor correlation is due to the fact that the quantitative measures only show the amount of error in the resultant image, not an evaluation of the type of image degradation. That is to say that the measure "does not adequately 'mimic' what the human visual system does in assessing image quality (Nill, p. 552)." As a result there has been an effort to find a quantitative measure that incorporates a model of the Human Visual System (HVS). The HVS model Nill defines is the function shown as equation 24 above and is used for the NAE and NMSE as previously described.

4. Graphical Techniques

a. Histogram

Histograms are best used to describe the error in the reconstructed image. There are several versions of histograms. First is the Difference Histogram. The Difference Histogram is constructed by first generating a difference image (subtracting the reconstructed pixel values from the corresponding value in the original image). The distribution of the pixel values in the difference image are then plotted. Typically, the distribution resembles a Gaussian distribution with higher fidelity images showing a spike at x=0.

Other types of Histograms are based on standard statistical measures; Standard Deviation, Skew and Kurtosis. The Standard Deviation Histogram is "based on the collected standard deviations from each original pixel histogram (Beser, p. 296)." The Skew Histogram "is a measure of the departure from symmetry (Beser, p. 296)." Large positive values show that the majority of pixels in the reconstructed image are above the average pixel value while large negative values show the opposite. Finally, the Kurtosis Histogram "is a measure of the peakness of the reconstructed image histogram (Beser, p. 296)." A large value represents a small slope in the reconstructed image histogram; a small value represents a large slope (i.e., a peak) in the reconstructed image histogram.

b. Hosaka Plot

Hosaka plots are intended to better reflect the human process of making a subjective evaluation on a particular image. Rather than comparing individual pixel values between the original and reconstructed image, particular image features are compared. The process for creating a Hosaka plot is relatively simple. The original image is segmented into NxN blocks where N is a power of 2. For each of these blocks, the variance is calculated. If the variance is greater than some predetermined threshold and the block size is greater than 1, the block is subdivided into 4 equally sized sub-blocks. The variance is again calculated and the process is repeated until the variance

of each block is less than the threshold. Once this process is completed, all blocks of size k are grouped together to form a class k where k=1,2,4,...,N. (Farrelle, p. 105)

The mean (Equation 37) and the standard deviation (Equation 38) of the nth block of each class are determined by:

(33) $\mu_k(n) = \frac{1}{k^2} \sum_{i=1}^{k} \sum_{j=1}^{k} u(i,j)$ for n=1,2,...,n_k *(Farrelle, p. 104)*

(34) $\sigma_k(n) = \sqrt{\frac{1}{k^2} \sum_{i=1}^{k} \sum_{j=1}^{k} [u(i,j) - \mu_k(n)]^2}$ for n=1,2,...,n_k *(Farrelle, p. 104)*

Once these have been calculated, the first feature (dm_k, Equation 41) is calculated for both the original and reconstructed images from the average class mean (Equation 39) and the average of the block means (Equation 40).

(35) $\bar{\mu}_k = \frac{1}{n_k} \sum_{n=1}^{n_k} \mu_k(n)$ where n_k is the number of blocks in the *k*th class. *(Farrelle, p. 104)*

(36) $m = \frac{1}{[\log_2 N+1]} [\bar{\mu}_1 + \bar{\mu}_2 + \bar{\mu}_4 + ... + \bar{\mu}_N]$ *(Farrelle, p. 105)*

This is generally not the same as the image mean unless each class has the same number of pixels.

(37) $dm_k = \bar{\mu}_k - m$ *(Farrelle, p. 105)*

Subtracting m from the average mean "removes the effects of dc drift which has no adverse effect on the perceived image quality (Farrelle, p. 105).

The other feature is the difference in the average standard deviation for each class (Equation 43). First the average standard deviation is calculated for the original and reconstructed image. The same block segmentation from the original image is used on the reconstructed image for determination of this standard deviation.

(38) $\bar{\sigma}_k = \frac{1}{n_k} \sum_{n=1}^{n_k} \sigma_k(n)$ *(Farrelle, p. 105)*

(39) $dS_k = |\bar{\sigma}_k - \bar{\sigma}_k^*|$ *(Farrelle, p. 106)*

(40) $dM_k = |dm_k - dm_k^*|$ *(Farrelle, p.106)*

where the * represents the value in the reconstructed image.

The Hosaka plot (an example is shown in Figure 5.1) is then created by plotting the dS and dM values on a polar plot where the radius is the feature value, dS vectors in the left half of the plane, dM vectors on the right half of the plane. The vectors are equally spaced for the different classes.

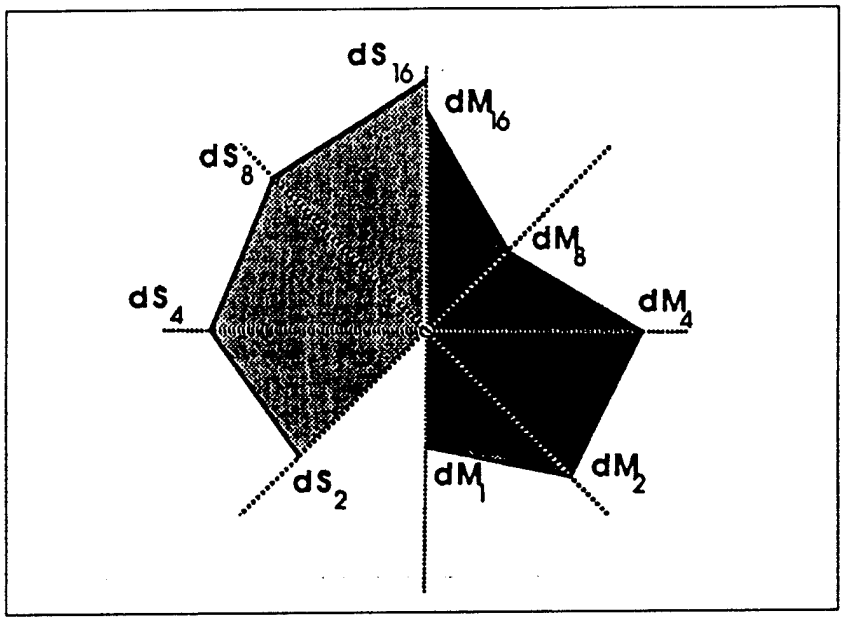

Figure 5.1 Sample Hosaka Plot (Farrelle, p. 107)

Farrelle uses three examples to demonstrate the utility of Hosaka plots. First, the addition of a dc shift to the original image to create the reconstructed image. The addition of this shift does not change the dS nor the dM values. As such the Hosaka plot would be a point at the origin. This makes intuitive sense in that the addition of 5, for example, to each pixel value would not change the relative difference between adjacent pixels and would therefore result in no decrease in subjective quality.

Second, the addition of noise causes the dS_k to have equal magnitudes proportional to the noise power. If the noise has a zero mean then the dM_k would be near zero since the means of class k would be the same and m would be unchanged. This case is shown in Figure 5.2.

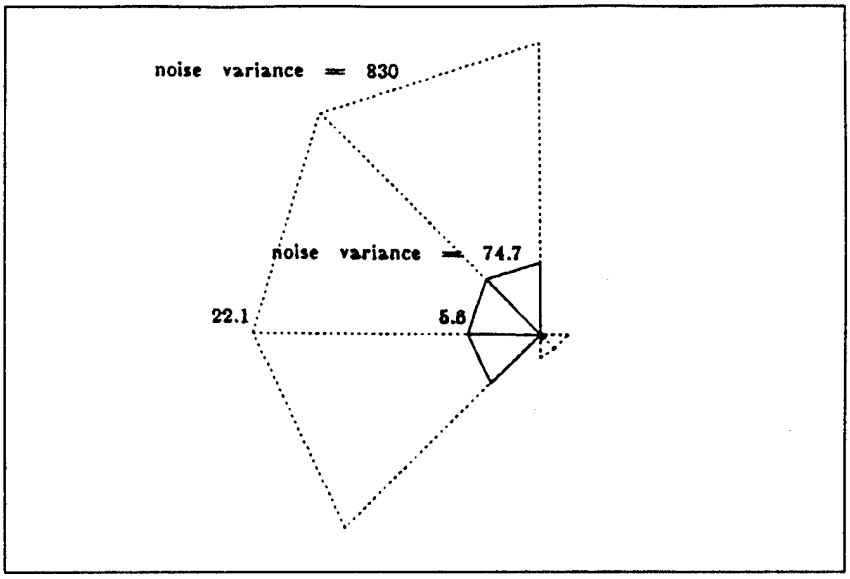

Figure 5.2 Hosaka Plot with added zero mean noise (Farrelle, p. 107)

The third case involves blurring the original image. In this case, the standard deviations (dS_k) would change for each class since the blurring would effect each class differently. Additionally, the means (dM_k) would also change for each class depending on the application of the blurriness. Figure 5.3 shows the effect of a single blurring function applied three times to an image.

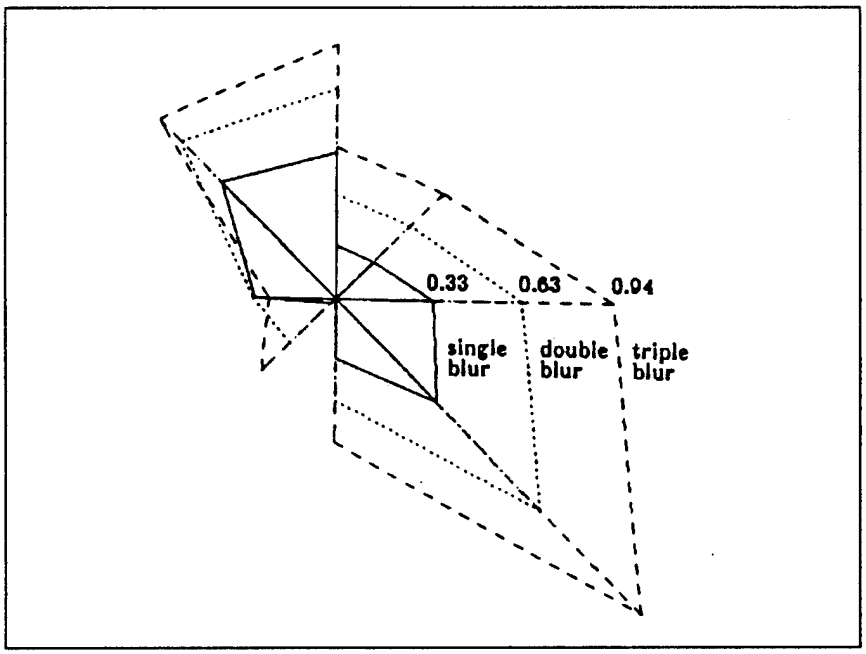

Figure 5.3 Hosaka Plot for blurred images (Farrelle, p. 109)

B. SUBJECTIVE MEASURES

1. Typical Subjective Evaluation

Subjective evaluations of imagery are just as the name implies, subjective. The evaluation of imagery using subjective measures is not a statistical technique but a psychological experiment and highly dependent on several factors:

- the Experience Base of the Observer
- the Experiment Design
- the Facilities (i.e., Lighting, Display, Room Environment, etc.)
- Application Data Set Selection (Selection of Relevant Data) and
- Compression Technique Parameter Selection (i.e., the "Tuning" of algorithms for optimum performance)

As such, these factors if not carefully controlled can invalidate the results of the subjective evaluation. (Beser, p. 294)

A typical subjective measure is computed as follows:

$$(41) \quad R = \frac{\left(\sum_{k=1}^{n} s_k n_k\right)}{\left(\sum_{k=1}^{n} n_k\right)} \qquad \textit{(Eskicioglu, Fisher and Chen, p. 55)}$$

where:

n is the number of grades in the scale

n_k is the number of observers that selected the particular rating

s_k is the score corresponding to the kth rating

Once calculated these values can be compared and a relative ranking of compression methods can be determined.

2. Subjective Evaluation Shown in this Thesis

This thesis takes a new approach at the subjective evaluation of imagery. It is based on the Analytic Hierarchy Process created by Thomas L. Saaty and described in detail in

his book The Analytic Hierarchy Process. A detailed description is contained in Appendix B and a complete discussion is contained in Saaty's book.

The gist of the Analytic Hierarchy Process is that pairwise comparisons are made between objects, in this case reconstructed imagery from various compression methods within one compression ratio. A matrix is constructed with the rating placed in matrix position (A, B) (A is the first image and B the second). At position (B,A), the reciprocal of the rating is entered. As the comparison of an image to itself should show equal quality, a value of 1 is placed along the diagonal. An example matrix is shown in Figure 5.4.

Image	A1	A2	A3	A4
A1	1	3	1/9	5
A2	1/3	1	7	1/3
A3	9	1/7	1	1
A4	1/5	3	1	1

Figure 5.4 Example AHP Matrix

Once the matrix is completed, a judgment vector is calculated by first normalizing the matrix along the columns and then averaging the values in each row. This closely approximates the principle eigenvector (the eigenvector associated with the largest eigenvalue) of the matrix. In the example matrix, the following judgment vector would result.

Compression Method	Value
1	0.302
2	0.246
3	0.281
4	0.171

Figure 5.5 Judgment Vector for Matrix in Figure 5.4

In this example the compression methods from best to worst would be: Method 1, Method 3, Method 2 and Method 4. Since this is a relative ranking, a comparison of the rankings can be made and an overall ranking can be determined.

VI. ANALYSIS

This analysis for this thesis was conducted using six different images. They were selected for specific tactical information as well as their ability to test the strengths and weaknesses of the algorithms (such as edges in the image). The images were selected from a variety of TARPS and Hand-Held Digital Camera images held by the Johns Hopkins University Applied Physics Laboratory. The six images are shown in Appendix A with the specific points chosen for image comparison annotated on each.

Each of the images was compressed using the following compression algorithms to four compression ratios (16:1, 32:1, 64:1, 128:1).

- Independent Standards Organization (ISO) Joint Photographic Experts Group (JPEG) (Except 128:1 since JPEG cannot compress to this ratio.)
- Aware Corporation Wavelet
- Yuval Fisher's Fractal Compression Program
- Navy TENCAP Radiant Tin (TID version 3.0)

A. QUANTITATIVE ANALYSIS

An Analysis of Variance (ANOVA) was conducted on each compression method at each compression ratio using the MINITAB statistical software. The raw data used for this analysis is contained in Appendix C. The ANOVA provides a p-value which is the smallest level of significance at which the hypothesis that the mean value for each statistic is the same. (i.e., $\mu_{jpeg} = \mu_{wavelet} = \mu_{fractal} = \mu_{tin}$). For this analysis a 95% confidence level was used for comparison. Thus, if the p-value for the measure exceeds 0.05, the hypothesis is accepted at the 95% confidence level meaning that there is no statistical difference among the compression methods using that measure. Otherwise the hypothesis is rejected and a ranking of the methods may be performed. The ANOVA p-Value results for 16:1, 32:1, 64:1 and 128:1 compression ratios are shown in Tables 6.1, 6.3, 6.5, and 6.7 respectively. The ranking of measures that have statistically

different means for the same compression ratios are shown in Tables 6.2, 6.4, 6.6 and 6.8 respectively.

1. **Results at the 16:1 Compression Ratio**

Quantitative Measure	p-value	Reject Hypothesis
AD	p=0.002	Yes
MD	p=0.001	Yes
LMSE	p=0.000	Yes
NAE (a)	p=0.748	No
NAE (b)	p=0.762	No
L_1	p=0.767	No
L_2	p=0.583	No
L_3	p=0.357	No
SC	p=0.000	Yes
NK	p=0.002	Yes
CQ	p=1.000	No
IF	p=0.495	No
PMSE	p=0.484	No
NMSE (a)	p=0.495	No
NMSE (b)	p=1.000	No
NMSE (c)	p=1.000	No

Table 6.1 ANOVA p-Values at 16:1 Compression Ratio

Ranking	AD	LMSE	MD
#1	Wavelet	Radiant Tin	Wavelet
#2	JPEG	Fractal	Radiant Tin
#3	Radiant Tin	JPEG	JPEG
#4	Fractal	Wavelet	Fractal

Ranking	SC	NK
#1	Wavelet	Wavelet
#2	JPEG	JPEG
#3	Radiant Tin	Radiant Tin
#4	Fractal	Fractal

Table 6.2 Ranking of Measures that have Statistically Different Means

2. Results at the 32:1 Compression Ratio

Quantitative Measure	p-value	Reject Hypothesis
AD	p=0.069	No
MD	p=0.033	Yes
LMSE	p=0.000	Yes
NAE (a)	p=0.403	No
NAE (b)	p=0.432	No
L_1	p=0.414	No
L_2	p=0.243	No
L_3	p=0.143	No
SC	p=0.000	Yes
NK	p=0.002	Yes
CQ	p=1.000	No
IF	p=0.121	No
PMSE	p=0.117	No
NMSE (a)	p=0.121	No
NMSE (b)	p=1.000	No
NMSE (c)	p=1.000	No

Table 6.3 ANOVA p-Values at 32:1 Compression Ratio

Ranking	MD	LMSE	SC	NK
#1	Wavelet	Fractal	JPEG	Wavelet
#2	Radiant Tin	Radiant Tin	Wavelet	JPEG
#3	JPEG	JPEG	Radiant Tin	Radiant Tin
#4	Fractal	Wavelet	Fractal	Fractal

Table 6.4 Ranking of Measures that have Statistically Different Means

3. Results at the 64:1 Compression Ratio

Quantitative Measure	p-value	Reject Hypothesis
AD	p=0.073	No
MD	p=0.061	No
LMSE	p=0.000	Yes
NAE (a)	p=0.065	No
NAE (b)	p=0.067	No
L_1	p=0.048	Yes
L_2	p=0.053	No
L_3	p=0.055	No
SC	p=0.005	Yes
NK	p=0.012	Yes
CQ	p=0.999	No
IF	p=0.029	Yes
PMSE	p=0.023	Yes
NMSE (a)	p=0.029	Yes
NMSE (b)	p=0.999	No
NMSE (c)	p=1.000	No

Table 6.5 ANOVA p-Values at 64:1 Compression Ratio

Ranking	SC	LMSE	L1	NK
#1	Wavelet	Fractal	Wavelet	Wavelet
#2	Radiant Tin	Radiant Tin	Radiant Tin	Radiant Tin
#3	JPEG	JPEG	Fractal	JPEG
#4	Fractal	Wavelet	JPEG	Fractal

Ranking	IF	PMSE	NMSE(a)
#1	Wavelet	Radiant Tin	Wavelet
#2	Fractal	Wavelet	Radiant Tin
#3	JPEG	JPEG	JPEG
#4	Radiant Tin	Fractal	Fractal

Table 6.6 Ranking of Measures that have Statistically Different Means

4. Results at the 128:1 Compression Ratio

Quantitative Measure	p-value	Reject Hypothesis
AD	p=0.627	No
MD	p=0.560	No
LMSE	p=0.000	Yes
NAE (a)	p=0.173	No
NAE (b)	p=0.235	No
L_1	p=0.144	Yes
L_2	p=0.090	No
L_3	p=0.083	No
SC	p=0.002	Yes
NK	p=0.008	Yes
CQ	p=0.984	No
IF	p=0.048	Yes
PMSE	p=0.036	Yes
NMSE (a)	p=0.048	Yes
NMSE (b)	p=0.985	No
NMSE (c)	p=0.996	No

Table 6.7 ANOVA p-Values at 128:1 Compression Ratio

Ranking	SC	LMSE	L1	NK
#1	Wavelet	Fractal	Wavelet	Wavelet
#2	Radiant Tin	Radiant Tin	Radiant Tin	Radiant Tin
#3	Fractal	Wavelet	Fractal	Fractal

Ranking	IF	PMSE	NMSE(a)
#1	Wavelet	Wavelet	Wavelet
#2	Radiant Tin	Radiant Tin	Radiant Tin
#3	Fractal	Fractal	Fractal

Table 6.8 Ranking of Measures that have Statistically Different Means

B. QUALITATIVE ANALYSIS

There were 11 observers chosen from the Space Systems Operations Program students and staff at the Naval Postgraduate School and from the Radiant Tin project team at the Johns Hopkins University Applied Physics Laboratory. The images were viewed in pairs following the script outlined in Appendix D. Each image was printed on a transparency using a Kodak ColorEase printer and was viewed on a light table in an isolated environment. While the observer was not limited to the time taken for each comparison, the goal was to limit each experiment to no longer than 1.5 hours. This goal was met.

In order to provide some randomness to the decision process, the order of the pairings was changed among the different observers. Additionally, the highest ratios of compression were shown first so as to minimize the effects of a learning curve. Finally, the results were analyzed using the Analytic Hierarchy Process described in Appendix B. The individual observer results are shown in Tables 6.9, 6.11, 6.13 and 6.15. The Rankings at each compression ratio are shown in Tables 6.10, 6.12, 6.14 and 6.16.

1. Results at 16:1 Compression Ratio

	JPEG	Wavelet	Fractal	Radiant Tin
Observer 1	0.29369	0.35122	0.13889	0.2162
Observer 2	0.30817	0.37544	0.1544	0.16199
Observer 3	0.29075	0.38221	0.1218	0.20524
Observer 4	0.28698	0.26962	0.23767	0.20573
Observer 5	0.29583	0.28194	0.20694	0.21528
Observer 6	0.2697	0.2697	0.23636	0.22424
Observer 7	0.34484	0.31098	0.15013	0.19405
Observer 8	0.33793	0.36513	0.10969	0.18725
Observer 9	0.26875	0.26875	0.23542	0.22708
Observer 10	0.29281	0.29107	0.19871	0.21741
Observer 11	0.29004	0.30604	0.21248	0.19144
Average	0.29813	0.31565	0.18205	0.20417

Table 6.9 Individual Observer Results at 16:1 Compression Ratio

Ranking	Method
#1	Wavelet
#2	JPEG
#3	Radiant Tin
#4	Fractal

Table 6.10 Ranking at 16:1 Compression Ratio

2. Results at 32:1 Compression Ratio

	JPEG	Wavelet	Fractal	Radiant Tin
Observer 1	0.21605	0.4574	0.07127	0.25528
Observer 2	0.30598	0.42541	0.07861	0.19001
Observer 3	0.32295	0.37594	0.04456	0.25655
Observer 4	0.29033	0.37328	0.11499	0.2214
Observer 5	0.33369	0.30336	0.0884	0.27455
Observer 6	0.25481	0.33933	0.09793	0.30793
Observer 7	0.26166	0.39473	0.07569	0.26792
Observer 8	0.21095	0.45084	0.05258	0.28563
Observer 9	0.2437	0.30468	0.20889	0.24272
Observer 10	0.27418	0.32857	0.14263	0.25463
Observer 11	0.2328	0.36774	0.10004	0.29942
Average	0.26792	0.37466	0.09778	0.25964

Table 6.11 Individual Observer Results at 32:1 Compression Ratio

Ranking	Method
#1	Wavelet
#2	JPEG
#3	Radiant Tin
#4	Fractal

Table 6.12 Ranking at 32:1 Compression Ratio

3. Results at 64:1 Compression Ratio

	JPEG	Wavelet	Fractal	Radiant Tin
Observer 1	0.085	0.44999	0.07406	0.39094
Observer 2	0.11717	0.45969	0.05942	0.36372
Observer 3	0.13401	0.44136	0.04862	0.37601
Observer 4	0.0958	0.48564	0.07321	0.34535
Observer 5	0.1228	0.52255	0.0761	0.27854
Observer 6	0.13799	0.43342	0.05954	0.36905
Observer 7	0.09609	0.49415	0.07317	0.33659
Observer 8	0.1147	0.45603	0.05435	0.37492
Observer 9	0.11894	0.43063	0.06813	0.3823
Observer 10	0.12638	0.4194	0.08314	0.37109
Observer 11	0.08842	0.46627	0.06297	0.38234
Average	0.11248	0.45992	0.06661	0.36099

Table 6.13 Individual Observer Results at 64:1 Compression Ratio

Ranking	Method
#1	Wavelet
#2	Radiant Tin
#3	JPEG
#4	Fractal

Table 6.14 Ranking at 64:1 Compression Ratio

4. Results at 128:1 Compression Ratio

	Wavelet	Fractal	Radiant Tin
Observer 1	0.55541	0.0606	0.38399
Observer 2	0.60066	0.06861	0.33073
Observer 3	0.52765	0.07529	0.39706
Observer 4	0.49222	0.09061	0.41717
Observer 5	0.42887	0.08716	0.48398
Observer 6	0.51364	0.08731	0.39905
Observer 7	0.4911	0.09457	0.41433
Observer 8	0.51845	0.07347	0.40808
Observer 9	0.49612	0.12031	0.38357
Observer 10	0.41296	0.11349	0.47355
Observer 11	0.50823	0.08117	0.41061
Average	0.50412	0.0866	0.40928

Table 6.15 Individual Observer Results at 128:1 Compression Ratio

Ranking	Method
#1	Wavelet
#2	Radiant Tin
#3	Fractal

Table 6.16 Ranking at 128:1 Compression Ratio

5. Summary of Qualitative Experiment Results

A summary of the results of the qualitative experiment is shown graphically in Figure 6.1.

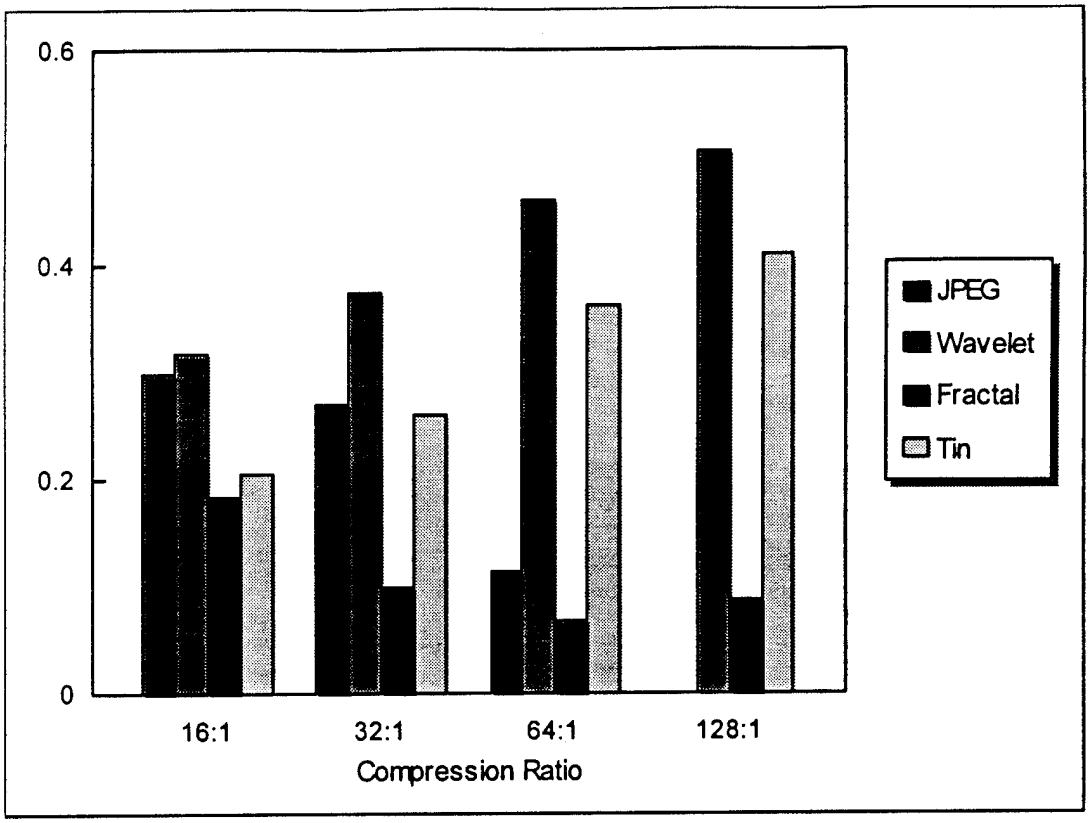

Figure 6.1 Summary of Qualitative Experiment Results

VII. CONCLUSIONS AND RECOMMENDATIONS

A. QUANTITATIVE VS. QUALITATIVE MEASURES

The quantitative analysis in Chapter VI shows that several measures are not useful for rating compression methods in that the values of the measures show no statistical difference. This is consistent with previous work specifically mentioned in Eskicioglu, Fisher, and Chen. They have stated that quantitative measures, in general, can "reliably be used to specify the magnitude of degradation in reconstructed images for a given compression technique." For those measures, however, which show statistical differences, the rankings roughly correspond to those obtained in the qualitative evaluation. As this thesis was a limited evaluation, this result in itself may be purely coincidence as "a single scalar value cannot be used to describe a variety of impairments (Eskicioglu, Fisher and Chen)." Since each compression method results in a different type of "impairment," it is not wise to base a judgment of compression methods on quantitative measures, particularly in the tactical environment where interpretability is typically independent of the quantitative error in the image.

The limited test set and number of observers used in the qualitative assessment provide a basis for ranking the compression methods. As shown previously in Figure 6.1, Wavelet compression appears to be the best choice of compression method across the various compression ratios. JPEG does very well at low ratios of compression as expected. Similarly, the Radiant Tin algorithm does very well at high ratios of compression. In the application of tactical imagery, fractal compression does not seem to be a good choice. One of the frequent comments that observers had after the experiment was that some of the images (which the experimenter determined to be those compressed using fractals) seemed to introduce features into the image which could possibly confuse the person interpreting the image. The most obvious was the introduction of additional aircraft in certain images. As fractal compression uses "pieces" of the original image for compression and subsequent reconstruction, it is probably not useful for this application.

B. RECOMMENDATIONS FOR FOLLOW-ON WORK

As stated above, this analysis was conducted on a limited test set with a limited number of observers. This test set consisted solely of visual imagery of similar content. Follow-on work would need to include imagery from other sensors (e.g., SAR and Thermal IR). One method of accomplishing this would be to gather imagery used in a tactical exercise and conduct the experiment on that imagery, as it should be an accurate reflection of the imagery required by a tactical commander.

Second, follow-on evaluations should include users from the field. As the requirement is to get imagery to disadvantaged users, they should be included in follow-on evaluations.

Finally, the platform used to compress/decompress imagery as well as the time to compress/decompress should be analyzed. The platform is important as units such as SEAL teams and Marine reconnaissance units that require imagery have limited resources (i.e., laptop Personal Computers at best) with which to work in the field. This is integrally related to the time for compression/decompression. As these units are particularly vulnerable, algorithms that compress/decompress faster than others and which provide reconstructed images of similar quality are clearly better.

APPENDIX A. TEST IMAGERY

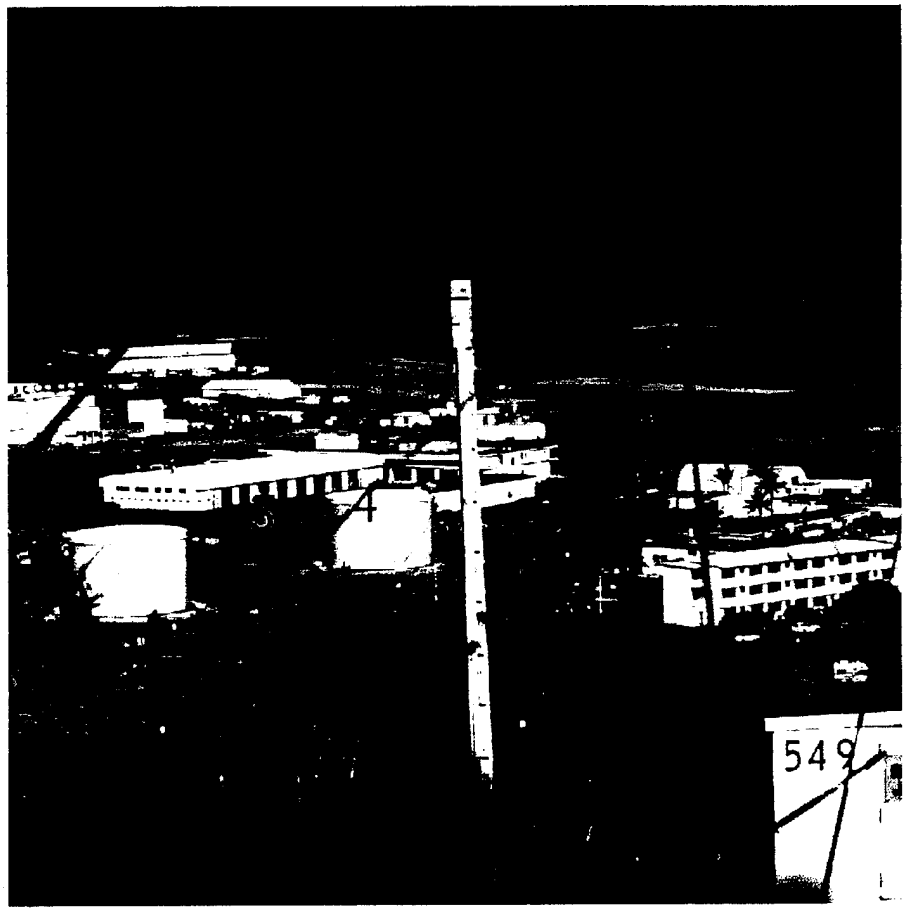

Figure A.1 Image 1 - npgford11

1. Airfield Control Tower
2. 4 Helicopters on Airstrip
3. HMMWV in front of Maintenance Building
4. Open/Closed Bay Doors on Maintenance Building
5. #549

Figure A.2 Image 2 - npglang3i

1. 6 White Aircraft
2. Buildings (edges)
3. Differentiate between Aircraft Type
4. Gray vs. White Aircraft
5. Count Cars

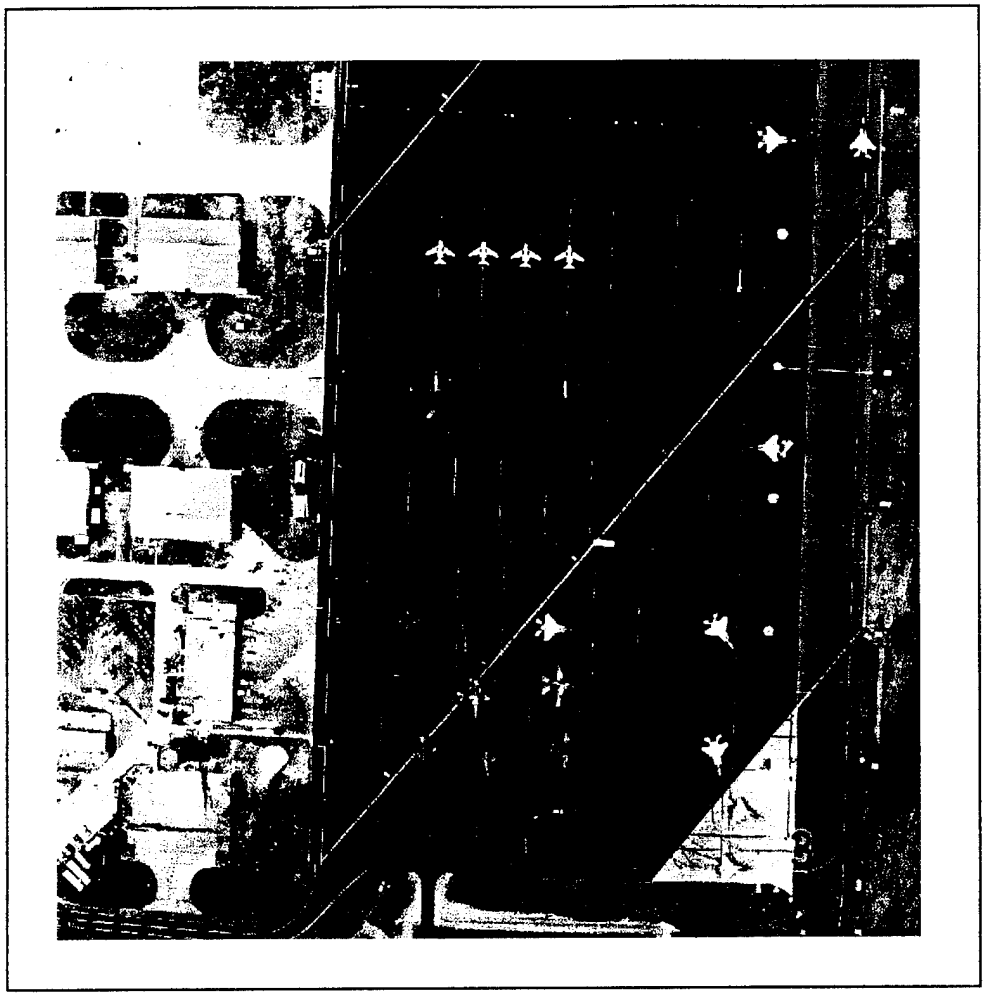

Figure A.3 Image 3 - npglang8i

1. Helicopters in Lower Left
2. Helicopter on Pad - Upper right
3. Aircraft in Lower Right (White on White)
4. APU Next to Aircraft
5. Training Aircraft
6. Differentiate between Aircraft Type

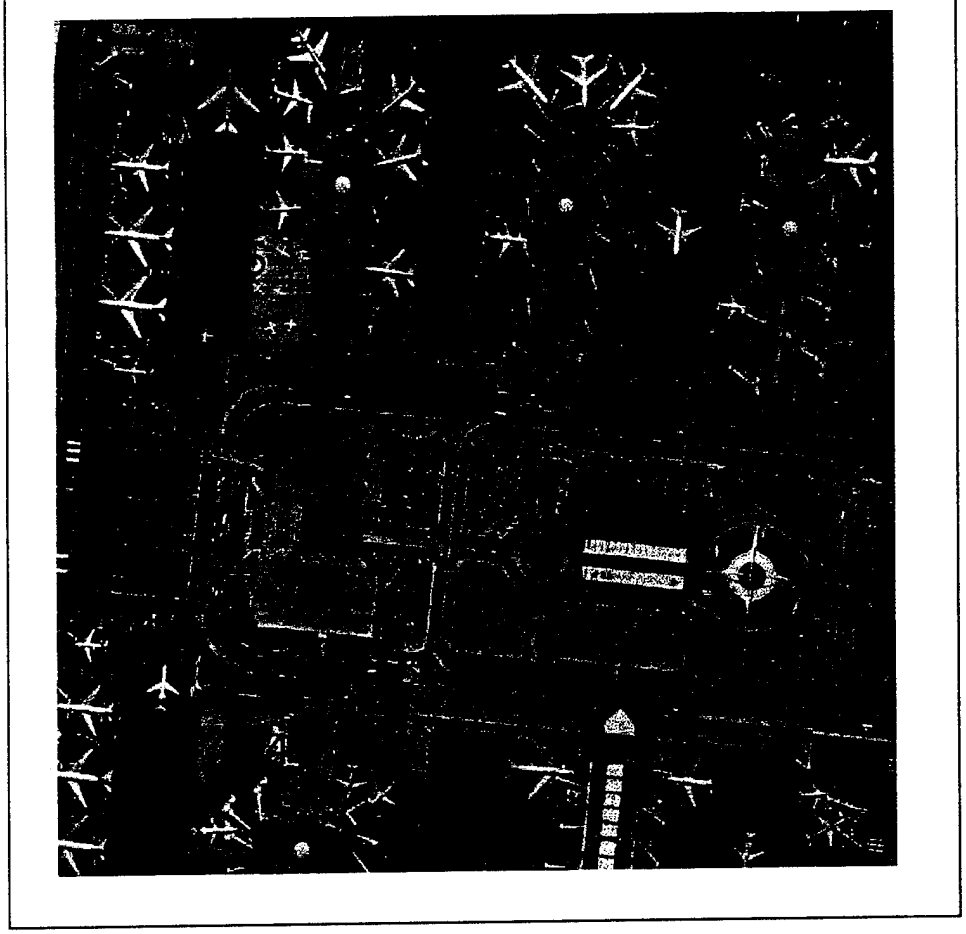

Figure A.4 Image 4 - npgLAX

1. Small Aircraft Right Side
2. Count Cars in Parking Lots
3. Buildings (Edges)
4. Terminal at Lower Left (Edges)
5. Small Aircraft Upper Left Terminal

Figure A.5 Image 5 - npgpalm

1. Aircraft Middle of Image
2. White Plane - Upper Left
3. Building with Half-Plane (edges)
4. Tank
5. Vehicles around Aircraft
6. Count Cars
7. Maintenance Buildings

Figure A.6 Image 6 - npgslangn10

1. Hull Number
2. Submarines
3. Cranes
4. Buildings at Head of Pier (edges)
5. Flight Deck Status
6. Differentiate Ship Types

APPENDIX B. THE ANALYTIC HIERARCHY PROCESS

The Analytic Hierarchy Process (AHP) was developed by Thomas L. Saaty to solve complex problems involving multiple criteria. It is designed specifically to deal with subjective evaluations of the relative importance of each of the criteria as well as the individual alternatives within each criterion. AHP provides a prioritized evaluation of problem. This evaluation not only shows which set of criteria provides the optimal solution but gives a relative weighting of the different sets. An example from Saaty is the easiest manner in which to describe the process. His example that begins in Section 1-6 of The Analytic Hierarchy Process will be followed.

First, it is essential that the problem be developed in a graphic representation showing the overall goal, the criteria and the decision alternatives. In the school selection problem, the overall goal is deciding on a school that provides the greatest satisfaction to the student making the decision. Six criteria were chosen as being the most important aspects of that choice: Learning, Friends, School Life, Vocational Training, College Preparation and Music Classes. The decision alternatives are schools A, B and C. This hierarchy is shown in Figure B.1.

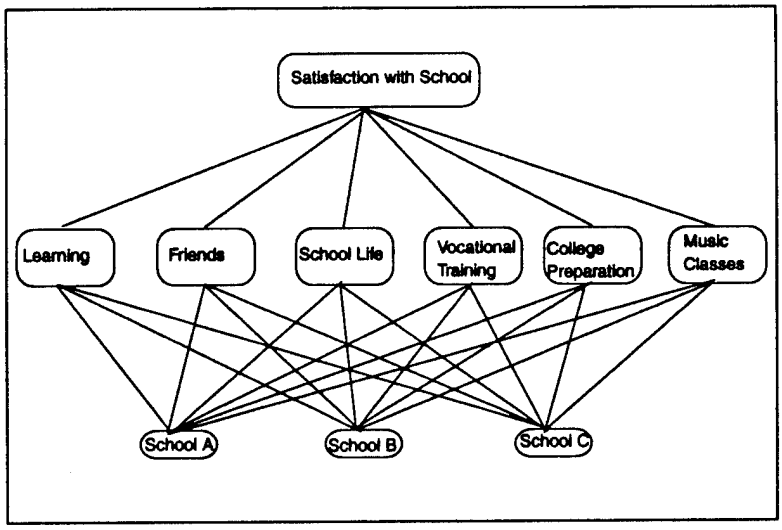

Figure B.1 School Satisfaction Hierarchy

Integral to the AHP is the determination of a matrix containing the results of pairwise comparison between the various alternatives within each criterion as well as the determination of a matrix similarly containing these results between the various criteria.

However, before pairwise comparisons can be made, it is essential that a subjective weighting scale be developed. Saaty supports a 9 level scale being the upper limit on size. These are based on 5 subjective attributes: equal, weak, strong, very strong, and absolute. This provides 5 levels with the additional 4 being the points in-between each attribute when greater precision is required. Various conversions of this scale are provided in Saaty's book.

The following ratings were used for the school example:

1 -- A and B are equally important

3 -- A is weakly more important than B

5 -- A is strongly more important than B

7 -- A is demonstrably more important than B

9 -- A is absolutely more important than B

Reciprocals of those ratings are used for the converse evaluation.

First pairwise comparisons are made between the various criteria. The results from the school selection example are in Table B.1.

The priority vector of this matrix is then determined. The priority vector is the normalized principle eigenvector (the eigenvector associated with the largest eigenvalue) of the matrix. Saaty describes two techniques which are good approximations of the priority vector. The one chosen for the development of this example is:

(1) Each column of the matrix is normalized

(2) Each row of the normalized matrix is averaged giving the priority vector.

For this example the normalized matrix is shown in Table B.2 and the priority vector of this matrix is shown in Table B.3.

	Learning	Friends	School Life	Vocational Training	College Preparation	Music Classes
Learning	1	4	3	1	3	4
Friends	1/4	1	7	3	1/5	1
School Life	1/3	1/7	1	1/5	1/5	1/6
Vocational Training	1	1/3	5	1	1	1/3
College Preparation	1/3	5	5	1	1	3
Music classes	1/4	1	6	3	1/3	1

Table B.1 Pairwise Comparisons between Criteria

	Learning	Friends	School Life	Vocational Training	College Preparation	Music Classes
Learning	0.32	0.35	0.11	0.11	0.52	0.42
Friends	0.08	0.09	0.26	0.33	0.04	0.11
School Life	0.11	0.01	0.04	0.02	0.04	0.02
Vocational Training	0.32	0.03	0.19	0.11	0.17	0.04
College Preparation	0.11	0.44	0.19	0.11	0.17	0.32
Music classes	0.08	0.09	0.22	0.33	0.06	0.11

Table B.2 Normalized Pairwise Comparisons between Criteria

	Value
Learning	0.31
Friends	0.15
School Life	0.04
Vocational Training	0.14
College Preparation	0.22
Music classes	0.15

Table B.3 Priority Vector of the Criteria Matrix

If the decision were to choose which criterion was most important, in this example, Learning is most important followed in order by College Preparation, Friends/Music Classes, Vocational Training and School Life. This example continues in that the decision is to choose among three schools. As such each of the schools must be compared against the others with respect to the individual criteria. Figure B.2 shows these matrices.

	Learning		
	A	B	C
A	1	1/3	1/2
B	3	1	3
C	2	1/3	1

	Friends		
	A	B	C
A	1	1	1
B	1	1	1
C	1	1	1

	School Life		
	A	B	C
A	1	5	1
B	1/5	1	1/5
C	1	5	1

	Vocational Training		
	A	B	C
A	1	9	7
B	1/9	1	1/5
C	1/7	5	1

	College Preparation		
	A	B	C
A	1	1/2	1
B	2	1	2
C	1	1/2	1

	Music Classes		
	A	B	C
A	1	6	4
B	1/6	1	1/3
C	1/4	3	1

Figure B.2 Pairwise Comparisons between Alternatives within each Criterion

The vectors of priority for each of the matrices contained in Figure B.2 are shown below.

School	Learning	Friends	School Life	Vocational Training	College Preparation	Music Classes
A	0.16	0.33	0.45	0.75	0.25	0.69
B	0.59	0.33	0.09	0.06	0.5	0.09
C	0.25	0.33	0.46	0.19	0.25	0.22

Table B.4 Eigenvectors for each Criterion

Finally the priority vector in Table B.3 is multiplied by the matrix of priority vectors from Table B.4. The result being a vector of the overall ranking of each alternative with respect to the criteria. For this example:

School A = 0.38

School B = 0.37

School C = 0.25

One inherent problem in the AHP is that of consistency. Mathematically, if A is twice B and B is twice C then A is six times C. Unfortunately this does not hold up in subjective evaluations. It is very likely that while A is weakly better than B (value of 3) and B is strongly better than C (value of 5) that the person making the evaluations may find A to be absolutely better than C (value of 9). While 3 times 5 is clearly not 9, this does not invalidate the AHP procedure.

APPENDIX C. QUANTITATIVE MEASURES RAW DATA

Each of the following tables (Table C.1 through C.15) contain the quantitative measures for each image under each compression method and compression ratio. In the tables, the image is referred to by the following letter code:

A - npgford11

B - npglang3i

C - npglang8i

D - npgLAX

E - npgpalm

F - npgslangn10

The letters a, b and c refer to the options discussed in Chapter V.

Image	A	B	C	D	E	F
AD	0.04611	-0.06959	0.00249	-0.019	-0.04509	0.00218
MD	62	115	80	56	77	25
LMSE	0	0	0	0	0	0
NAE (a)	0.02351	0.03987	0.03979	0.05273	0.05291	0.01636
NAE (b)	0.00886	0.01644	0.01719	0.01835	0.01911	0.00564
NAE (c)	1	1	1	1	1	1
L1	2.66938	6.31068	5.23492	6.75567	7.56444	2.62771
L2	4.08956	9.26046	7.54321	8.69939	9.79656	3.39337
L3	5.68598	12.4558	10.0802	10.4365	11.8423	4.04675
SC	1.00134	1.00039	1.00103	1.00137	1.00126	1.00014
NK	0.99882	0.99832	0.99822	0.99713	0.99715	0.99972
CQ	144.916	182.409	170.656	134.649	150.782	169.062
IF	0.99898	0.99703	0.99747	0.99563	0.99556	0.99958
PMSE	0.00026	0.00132	0.00088	0.00129	0.00152	0.00018
NMSE (a)	0.00102	0.00297	0.00253	0.00437	0.00444	0.00042
NMSE (b)	671.693	947.947	845.448	633.331	740.807	865.099
NMSE (c)	245.238	220.476	210.655	195.886	201.485	368.042

Table C.1 JPEG Compression, 16:1 Compression Ratio

Image	A	B	C	D	E	F
AD	0.06002	-0.00551	0.01812	0.01466	-0.00457	0.00543
MD	31	56	52	48	58	19
LMSE	0.25803	0.42361	0.33849	0.74566	0.76274	0.49426
NAE (a)	0.01935	0.0348	0.03566	0.05014	0.04959	0.01461
NAE (b)	0.00744	0.01409	0.01534	0.01745	0.01784	0.00505
NAE (c)	1	1	1	1	1	1
L1	2.19665	5.50731	4.69127	6.42412	7.09013	2.34594
L2	3.15802	7.54196	6.35829	8.1801	9.04165	3.01701
L3	4.0875	9.47856	7.98052	9.69155	10.737	3.5715
SC	1.00182	1.00016	1.00044	1.00129	1.00102	1.00018
NK	0.99879	0.99894	0.99888	0.99742	0.9976	0.99974
CQ	144.911	182.521	170.769	134.689	150.85	169.066
IF	0.99939	0.99803	0.9982	0.99613	0.99622	0.99966
PMSE	0.00015	0.00087	0.00062	0.00114	0.0013	0.00014
NMSE (a)	0.00061	0.00197	0.0018	0.00387	0.00378	0.00034
NMSE (b)	671.354	948.176	845.962	633.391	741.001	865.062
NMSE (c)	245.13	220.536	210.784	195.909	201.54	368.028

Table C.2 Wavelet Compression, 16:1 Compression Ratio

Image	A	B	C	D	E	F
AD	0.08787	0.17295	0.15951	0.16335	0.13594	0.14561
MD	91	141	129	99	126	58
LMSE	0	0	0	0	0	0
NAE (a)	0.03349	0.0427	0.04359	0.06364	0.06117	0.0185
NAE (b)	0.01303	0.01669	0.01809	0.02206	0.02178	0.00641
NAE (c)	1	1	1	1	1	1
L1	3.8014	6.75793	5.7347	8.15326	8.7461	2.97084
L2	5.79745	10.0388	8.60723	10.8137	11.4776	3.86683
L3	8.1519	13.9868	12.1614	13.4605	14.2288	4.68186
SC	1.00555	1.00731	1.00755	1.01222	1.00987	1.00265
NK	0.99622	0.99463	0.99461	0.99058	0.99207	0.99841
CQ	144.539	181.734	170.038	133.765	150.014	168.84
IF	0.99796	0.99652	0.99671	0.99324	0.99391	0.99945
PMSE	0.00052	0.00155	0.00114	0.002	0.00209	0.00023
NMSE (a)	0.00204	0.00348	0.00329	0.00676	0.00609	0.00055
NMSE (b)	668.742	941.167	839.738	626.166	734.179	862.855
NMSE (c)	244.211	218.97	209.291	193.79	199.776	367.129

Table C.3 Fractal Compression, 16:1 Compression Ratio

Image	A	B	C	D	E	F
AD	0.28945	0.03293	-0.01288	0.00442	0.00501	0.08037
MD	36	71	57	58	58	19
LMSE	0	0	0	0	0	0
NAE (a)	0.0255	0.03878	0.03938	0.0557	0.05386	0.01637
NAE (b)	0.00972	0.01559	0.01676	0.01934	0.01934	0.00565
NAE (c)	1	1	1	1	1	1
L1	2.89448	6.13693	5.18095	7.13633	7.70094	2.62851
L2	4.13774	8.44207	7.01444	9.17395	9.85196	3.35242
L3	5.30163	10.6419	8.76694	10.9786	11.7321	3.94702
SC	1.00666	1.00276	1.0025	1.00374	1.00447	1.00124
NK	0.99617	0.99739	0.99766	0.9957	0.99553	0.99917
CQ	144.531	182.239	170.56	134.457	150.537	168.97
IF	0.99896	0.99754	0.99781	0.99514	0.99551	0.99959
PMSE	0.00026	0.0011	0.00076	0.00144	0.00154	0.00017
NMSE (a)	0.00104	0.00246	0.00219	0.00486	0.00449	0.00041
NMSE (b)	667.998	945.612	844.132	631.747	738.31	864.118
NMSE (c)	243.951	219.957	210.344	195.423	200.837	367.646

Table C.4 Radiant Tin Compression, 16:1 Compression Ratio

Image	A	B	C	D	E	F
AD	0.09099	0.0878	-0.01804	-0.15903	-0.03557	-0.14196
MD	88	141	137	88	102	34
LMSE	0	0	0	0	0	0
NAE (a)	0.04236	0.05192	0.05473	0.07018	0.06531	0.0212
NAE (b)	0.01625	0.02122	0.02341	0.02434	0.02367	0.00725
NAE (c)	1	1	1	1	1	1
L1	4.80904	8.21721	7.20003	8.99141	9.33874	3.40359
L2	7.14548	12.0362	10.485	11.8059	12.2436	4.43952
L3	9.70208	16.2355	14.0771	14.4376	14.9768	5.37698
SC	1.00366	1.00286	1.00124	0.99982	1.0022	0.99868
NK	0.99663	0.99607	0.99694	0.99606	0.99544	1.0003
CQ	144.597	181.997	170.437	134.505	150.523	169.16
IF	0.9969	0.99499	0.99511	0.99194	0.99307	0.99927
PMSE	0.00079	0.00223	0.00169	0.00238	0.00238	0.0003
NMSE (a)	0.0031	0.00501	0.00489	0.00806	0.00693	0.00073
NMSE (b)	670.079	945.554	845.286	634.371	740.103	866.411
NMSE (c)	244.67	219.925	210.596	196.191	201.299	368.583

Table C.5 JPEG Compression, 32:1 Compression Ratio

Image	A	B	C	D	E	F
AD	0.11808	0.03843	0.02785	-0.00835	0.01328	0.00061
MD	57	118	103	67	89	28
LMSE	0.52731	0.63994	0.58203	0.86276	0.87513	0.54404
NAE (a)	0.02935	0.04402	0.04743	0.05992	0.05816	0.01816
NAE (b)	0.01103	0.01796	0.0202	0.0208	0.02105	0.00625
NAE (c)	1	1	1	1	1	1
L1	3.33195	6.96678	6.23948	7.6764	8.31547	2.91537
L2	5.15628	10.0125	8.96184	10.0098	10.8315	3.77203
L3	7.07488	13.1805	11.8193	12.1547	13.1645	4.518
SC	1.00388	1.00161	1.00092	1.00292	1.00292	1.00027
NK	0.99726	0.99746	0.99775	0.99565	0.99583	0.99961
CQ	144.69	182.252	170.576	134.449	150.583	169.043
IF	0.99839	0.99653	0.99643	0.99421	0.99457	0.99948
PMSE	0.00041	0.00154	0.00124	0.00171	0.00186	0.00022
NMSE (a)	0.00161	0.00347	0.00357	0.00579	0.00543	0.00052
NMSE (b)	669.92	946.761	845.562	632.301	739.535	864.988
NMSE (c)	244.615	220.21	210.682	195.579	201.148	367.995

Table C.6 Wavelet Compression, 32:1 Compression Ratio

Image	A	B	C	D	E	F
AD	0.04306	0.10269	0.14653	0.10135	0.01874	0.12661
MD	141	190	192	123	126	62
LMSE	0	0	0	0	0	0
NAE (a)	0.05497	0.05992	0.06145	0.08723	0.07862	0.02255
NAE (b)	0.02139	0.02308	0.02489	0.03009	0.02818	0.00769
NAE (c)	1	1	1	1	1	1
L1	6.24039	9.48354	8.08384	11.1752	11.2412	3.62155
L2	9.57968	14.4027	13.0951	15.1255	14.9955	4.81904
L3	13.0444	20.3199	19.5638	19.0001	18.7409	5.99765
SC	1.00981	1.01057	1.01131	1.019	1.0131	1.00276
NK	0.99236	0.99118	0.9906	0.98407	0.98833	0.9982
CQ	143.978	181.105	169.352	132.885	149.449	168.804
IF	0.99443	0.99283	0.99238	0.98678	0.9896	0.99914
PMSE	0.00141	0.00319	0.00264	0.00391	0.00357	0.00036
NMSE (a)	0.00557	0.00717	0.00762	0.01322	0.0104	0.00086
NMSE (b)	665.784	938.005	836.507	621.767	731.711	862.748
NMSE (c)	243.179	218.258	208.505	192.498	199.136	367.086

Table C.7 Fractal Compression, 32:1 Compression Ratio

Image	A	B	C	D	E	F
AD	0.17322	0.02137	-0.00087	0.02189	-0.01898	0.08056
MD	70	108	92	80	87	28
LMSE	0	0	0	0	0	0
NAE (a)	0.03775	0.04728	0.05051	0.06612	0.06229	0.01958
NAE (b)	0.01408	0.01907	0.02116	0.0229	0.02249	0.00672
NAE (c)	1	1	1	1	1	1
L1	4.28554	7.48226	6.64461	8.47063	8.90696	3.14364
L2	6.51999	10.7464	9.45786	11.1598	11.6274	4.05133
L3	8.79462	14.1232	12.4008	13.6678	14.1342	4.83097
SC	1.00726	1.00328	1.00392	1.00532	1.00552	1.00147
NK	0.99511	0.99637	0.99606	0.99376	0.99413	0.99897
CQ	144.377	182.053	170.286	134.194	150.325	168.934
IF	0.99742	0.99601	0.99602	0.9928	0.99375	0.9994
PMSE	0.00065	0.00178	0.00138	0.00213	0.00215	0.00025
NMSE (a)	0.00258	0.00399	0.00398	0.0072	0.00625	0.0006
NMSE (b)	667.563	945.116	842.899	630.716	737.509	863.911
NMSE (c)	243.79	219.839	210.044	195.111	200.624	367.564

Table C.8 Radiant Tin Compression, 32:1 Compression Ratio

Image	A	B	C	D	E	F
AD	0.64086	0.76596	0.33604	0.4462	0.55421	-0.50066
MD	168	192	194	156	160	68
LMSE	0	0	0	0	0	0
NAE (a)	0.10324	0.0792	0.0945	0.10404	0.09753	0.03399
NAE (b)	0.04121	0.0316	0.04011	0.03612	0.03527	0.01151
NAE (c)	1	1	1	1	1	1
L1	11.7197	12.5346	12.4317	13.3295	13.9451	5.45755
L2	15.3174	17.6699	16.9435	17.5307	18.1106	7.15103
L3	19.1191	23.5002	22.102	21.5188	22.165	8.78248
SC	1.00431	1.0146	1.00705	1.00816	1.0122	0.99466
NK	0.99073	0.98741	0.99012	0.98707	0.98639	1.00174
CQ	143.742	180.415	169.27	133.291	149.155	169.404
IF	0.98575	0.9892	0.98724	0.98224	0.98483	0.99812
PMSE	0.00361	0.0048	0.00441	0.00525	0.00521	0.00079
NMSE (a)	0.01425	0.0108	0.01276	0.01776	0.01517	0.00188
NMSE (b)	669.864	934.297	840.331	629.027	732.589	870.028
NMSE (c)	244.501	217.385	209.382	194.561	199.305	370.079

Table C.9 JPEG Compression, 64:1 Compression Ratio

Image	A	B	C	D	E	F
AD	0.21351	0.0459	0.04718	0.02282	-0.0259	0.014
MD	92	152	136	100	110	40
LMSE	0.71196	0.83905	0.83705	0.91498	0.91671	0.58169
NAE (a)	0.04097	0.05281	0.05906	0.07221	0.06719	0.02121
NAE (b)	0.01527	0.02156	0.02497	0.02505	0.02444	0.00725
NAE (c)	1	1	1	1	1	1
L1	4.65082	8.35885	7.76924	9.25168	9.60627	3.40642
L2	7.51532	12.5003	11.733	12.2598	12.7138	4.47254
L3	10.6732	17.0671	16.1479	15.0745	15.6835	5.44351
SC	1.00744	1.00335	1.00315	1.00368	1.00359	1.00056
NK	0.9946	0.99563	0.99537	0.99382	0.99447	0.99935
CQ	144.303	181.917	170.169	134.203	150.377	169
IF	0.99657	0.9946	0.99388	0.99131	0.99252	0.99926
PMSE	0.00087	0.0024	0.00212	0.00257	0.00257	0.00031
NMSE (a)	0.00343	0.0054	0.00612	0.00869	0.00748	0.00074
NMSE (b)	667.45	945.071	843.623	631.829	739.027	864.729
NMSE (c)	243.749	219.824	210.195	195.43	201.012	367.888

Table C.10 Wavelet Compression, 64:1 Compression Ratio

Image	A	B	C	D	E	F
AD	0.04128	0.11652	0.09075	-0.01366	0.06785	0.11802
MD	159	205	195	123	143	93
LMSE	0	0	0	0	0	0
NAE (a)	0.07787	0.07282	0.07508	0.11094	0.09541	0.02932
NAE (b)	0.0291	0.0278	0.0296	0.03817	0.03436	0.00979
NAE (c)	1	1	1	1	1	1
L1	8.84	11.5258	9.87669	14.2129	13.6414	4.70792
L2	13.917	17.6979	16.2522	19.3531	18.4443	6.5881
L3	19.1827	24.9585	24.2163	24.2218	23.292	8.58005
SC	1.01755	1.01443	1.01469	1.02532	1.01918	1.00353
NK	0.9855	0.98747	0.98689	0.97683	0.98272	0.99744
CQ	142.983	180.426	168.718	131.908	148.6	168.677
IF	0.98824	0.98917	0.98826	0.97835	0.98427	0.9984
PMSE	0.00298	0.00482	0.00406	0.0064	0.0054	0.00067
NMSE (a)	0.01176	0.01083	0.01174	0.02165	0.01573	0.0016
NMSE (b)	660.471	934.3	833.602	617.729	727.159	862.052
NMSE (c)	241.321	217.423	207.804	191.311	197.943	366.8

Table C.11 Fractal Compression, 64:1 Compression Ratio

Image	A	B	C	D	E	F
AD	0.25094	-0.01528	-0.03742	0.03882	-0.00492	0.02719
MD	106	146	138	103	96	50
LMSE	0	0	0	0	0	0
NAE (a)	0.04893	0.05623	0.06153	0.0768	0.0701	0.02321
NAE (b)	0.01802	0.02269	0.0256	0.02655	0.0254	0.00787
NAE (c)	1	1	1	1	1	1
L1	5.55501	8.89908	8.09459	9.83887	10.0232	3.72678
L2	8.69094	13.2563	12.0334	13.2232	13.3034	4.96885
L3	12.022	18.1218	16.4577	16.4839	16.439	6.15677
SC	1.01047	1.00357	1.00521	1.00708	1.00713	1.00108
NK	0.99253	0.99518	0.99419	0.99143	0.99237	0.99901
CQ	144.003	181.835	169.966	133.88	150.059	168.941
IF	0.99541	0.99392	0.99356	0.98989	0.99181	0.99909
PMSE	0.00116	0.0027	0.00223	0.00299	0.00281	0.00038
NMSE (a)	0.00459	0.00608	0.00644	0.01011	0.00819	0.00091
NMSE (b)	665.353	944.842	841.782	629.572	736.288	864.252
NMSE (c)	243.01	219.77	209.771	194.769	200.3	367.685

Table C.12 Radiant Tin Compression, 64:1 Compression Ratio

Image	A	B	C	D	E	F
AD	0.26194	0.0216	0.04334	-0.02754	-0.05063	0.01297
MD	136	172	181	118	125	49
LMSE	0.81236	0.90136	0.90823	0.94418	0.93907	0.59838
NAE (a)	0.05575	0.06114	0.06933	0.08486	0.07642	0.02459
NAE (b)	0.02048	0.02489	0.02918	0.02938	0.02797	0.00831
NAE (c)	1	1	1	1	1	1
L1	6.32902	9.67614	9.12056	10.8717	10.927	3.94908
L2	10.4926	14.7697	14.0678	14.7239	14.7245	5.35838
L3	15.2786	20.5027	19.6256	18.3895	18.4561	6.73343
SC	1.01152	1.00471	1.00528	1.00653	1.00514	1.00082
NK	0.99097	0.99388	0.99297	0.99049	0.99243	0.99906
CQ	143.776	181.598	169.759	133.753	150.068	168.951
IF	0.99332	0.99246	0.9912	0.98747	0.98997	0.99894
PMSE	0.00169	0.00335	0.00304	0.0037	0.00344	0.00044
NMSE (a)	0.00668	0.00754	0.0088	0.01253	0.01003	0.00106
NMSE (b)	664.636	943.747	841.771	629.944	737.842	864.487
NMSE (c)	242.717	219.528	209.747	194.867	200.696	367.788

Table C.13 Wavelet Compression, 128:1 Compression Ratio

Image	A	B	C	D	E	F
AD	0.0298	0.04659	0.08617	0.00554	0.09143	0.07571
MD	162	202	202	126	149	93
LMSE	0	0	0	0	0	0
NAE (a)	0.09904	0.08564	0.08828	0.12321	0.10757	0.03524
NAE (b)	0.0357	0.03264	0.03412	0.04238	0.03883	0.01162
NAE (c)	1	1	1	1	1	1
L1	11.2437	13.554	11.6134	15.7857	15.3811	5.65931
L2	17.9786	20.9977	19.0584	21.3736	20.9075	8.14575
L3	24.7617	29.664	27.9343	26.4905	26.5037	10.7432
SC	1.02685	1.0188	1.01951	1.03049	1.02462	1.00398
NK	0.97711	0.98315	0.98236	0.972	0.97788	0.9968
CQ	141.766	179.637	167.943	131.256	147.868	168.568
IF	0.98038	0.98475	0.98385	0.97359	0.97978	0.99756
PMSE	0.00497	0.00678	0.00559	0.0078	0.00694	0.00102
NMSE (a)	0.01962	0.01525	0.01615	0.02641	0.02022	0.00244
NMSE (b)	654.187	930.132	829.5	614.472	723.126	861.644
NMSE (c)	239.136	216.484	206.827	190.35	196.888	366.636

Table C.14 Fractal Compression, 128:1 Compression Ratio

Image	A	B	C	D	E	F
AD	0.33169	0.08936	-0.02704	0.13259	0.0551	0.00517
MD	138	191	207	139	137	99
LMSE	0	0	0	0	0	0
NAE (a)	0.06384	0.06655	0.07286	0.10092	0.0789	0.0263
NAE (b)	0.02338	0.02672	0.0299	0.03479	0.02864	0.00885
NAE (c)	1	1	1	1	1	1
L1	7.24727	10.5322	9.58463	12.9302	11.2808	4.22329
L2	11.375	15.9695	14.765	17.6732	15.1798	5.75545
L3	15.8773	22.2794	20.8583	22.3526	19.0238	7.28389
SC	1.01471	1.00646	1.00674	1.0119	1.00968	1.00126
NK	0.98882	0.99238	0.99181	0.9851	0.98988	0.99876
CQ	143.465	181.324	169.559	133.024	149.682	168.9
IF	0.99214	0.99118	0.99031	0.98195	0.98934	0.99878
PMSE	0.00199	0.00392	0.00335	0.00533	0.00366	0.00051
NMSE (a)	0.00786	0.00882	0.00969	0.01805	0.01066	0.00122
NMSE (b)	662.456	942.056	840.484	626.475	734.36	864.09
NMSE (c)	241.986	219.133	209.443	193.844	199.792	367.62

Table C.15 Radiant Tin Compression, 128:1 Compression Ratio

APPENDIX D. QUALITATIVE EXPERIMENT SETUP

The script and a sample data collection sheet are provided in this appendix.

A. EXPERIMENT SCRIPT

The purpose of this experiment is to find the qualitative difference in a variety of images, compressed using 4 compression algorithms at 4 compression ratios.

I will be showing you 6 different images. You will be asked to compare the images for the ability to extract tactically relevant information from the images. The idea is not which image is aesthetically more pleasing but which is better for extracting the tactical information. The following scale will be used for this comparison.

Value	Observation Definition
9	Image is the only image from which the requested information can be exploited.
7	Image is significantly better for exploiting the requested information
5	Image is somewhat better for exploiting the requested information
3	Image is slightly better for exploiting the requested information
1	There is no difference between the images for exploiting the requested information

Here are the original 6 images and the tactical information that are specific items that may be used for this comparison:

npgford11 - This image was taken by a digital handheld camera of Ford Island, HI. Items to look for include:

- Airfield Control Tower
- 4 Helicopters on Airstrip
- HMMWV in front of Maintenance Building
- Open/Closed Bay Doors on Maintenance Building
- # 549

npglang3i - This image was taken by a TARPS imager of Langley Field. Items to look for include:

- Differentiate between Aircraft Type
- Grey vs. White Aircraft
- 6 White Aircraft
- Count Cars
- Buildings (Edges)

npglang8i - This image was taken by a TARPS imager of Langley Field. Items to look for include:

- Differentiate between Aircraft Type
- Helos in Lower Left
- Helo on Pad - Upper Right
- Aircraft in Lower Right (White on White)
- APU Next to Planes in Upper Left
- Training Aircraft 2nd Row

npgLAX - This image was taken by a TARPS imager of LAX. Items to look for include:

- Small Aircraft Right Side
- Cars in Parking Lots
- Buildings Bottom of Image
- Terminal at Lower Left
- Small Aircraft Upper Left Terminal

npgpalm - This image was taken by a TARPS imager of Palmdale Airport. Items to look for include:

- Aircraft Middle of Image
- White Plane - Upper Left
- Building with Half-plane

- Count Cars
- Tank
- Maintenance Buildings
- Vehicles around Aircraft

npgslangn10 - This image was taken by a TARPS imager of a Shipyard near Langley. Items to look for include:

- Which carrier (Hull number)
- Submarines Upper Left
- Cranes
- Flight Deck Status
- Differentiate Ship types
- Buildings at Head of Pier

Finally, after each set of comparisons you will be asked to assign a level of confidence to each individual image on your ability to extract the tactical information from the image compared to the original image. The following scale will be used:

Image Confidence	Description
0	I have no confidence in the ability to extract tactical information from the image
25	I have some confidence in the ability to extract tactical information from the image
50	I have moderate confidence in the ability to extract tactical information from the image
75	I have a high confidence in the ability to extract tactical information from the image.
100	I have full confidence in the ability to extract tactical information from the image

Additionally, in some cases the images you will be comparing are exactly the same. The purpose for this is for statistical control and please do not go out of your way to look

for these pairs. They are random and may or may not occur in the process of this test. Finally, again a reminder, the evaluation is to be made for which image is more useful for extracting the tactical information, not which is more aesthetically pleasing.

NOTE: After each compression ratio,

"Again a reminder, the evaluation is to be made for which image is more useful for extracting the tactical information, not which is more aesthetically pleasing."

B. DATA COLLECTION SHEET

The table below is an abstract of the collection sheet used for the qualitative experiment. Each image was randomly numbered to mask it's identity. The image pairs were created using a random number generator.

Image Name	Image A	Image B	Rating	Confidence Rating	
				Image	Rating
npgford11	57	39		39	
	85	57		57	
	85	39		85	
npglang3i	63	40		17	
	63	17		40	
	17	40		63	
npglang8i	64	82		109	
	64	109		64	
	109	82		82	
npgLAX	16	61		61	
	61	11		16	
	16	11		11	
npgpalm	87	110		42	
	110	42		87	
	42	87		110	
npgslangn10	74	28		88	
	88	28		28	
	74	88		74	

Table D.1 Example Data Collection Sheet

LIST OF REFERENCES

_____. *Military Standard 188-198A - Joint Photographics Expert Group (JPEG) Image Compression for the National Transmission Format.* 1993.

Beser, Nicholas D. Class Notes, JHU Data and Image Compression (605.769) Fall 1993. Johns Hopkins University APL. 1993.

Beser, Nicholas D. "Image Data Compression Metrics." AIAA-93-4513-CP. AIAA. pp. 292-303. 1993.

Beser, Nicholas D. "Space Data Compression Standards." *Johns Hopkins APL Technical Digest Vol. 15, No. 3.* Johns Hopkins University APL. Laurel, MD. pp. 206-223. 1994.

Boger, Dan and Carl Jones. Class Notes, NPS SS4002 Spring 1995. Naval Postgraduate School. 1995.

Cracknell, A.B. and L.W.B Hayes. *Introduction to Remote Sensing.* Taylor and Francis. London. 1991.

Elachi, Charles. *Introduction to the Physics and Techniques of Remote Sensing.* John Wiley and Sons. New York. 1987.

Eskicioglu, Ahmet M., Paul S. Fisher and Siyuan Chen. "Image Quality Measures and their Performance." *1994 Space and Earth Science Data Compression Workshop.* National Aeronautics and Space Administration. Greenbelt, MD. pp. 55-67. 1994.

Farrelle, Paul M. *Recursive Block Coding for Image Data Compression.* Springer-Verlag. New York. 1990.

Fisher, Yuval. *Fractal Image Compression.* Springer-Verlag. New York. 1995.

Gunston, Bill. *An Illustrated Guide to Spy Planes.* Prentice Hall Press. New York. 1983.

Huffman, David A. "A Method for the Construction of the Minimum-Redundancy Codes." *Proceedings of the IRE.* pp. 1098-1101. September, 1952.

ISOA, APL. "TID 3.0 Documentation." ISOA, APL. April, 1995.

Muolo, Michael J. *Space Handbook: A War Fighters Guide to Space.* Air University Press. Maxwell AFB, AL. 1993.

Nelson, Mark. *The Data Compression Book.* M&T Books. 1991.

Nill, Norman B. "A Visual Model Weighted Cosine Transform for Image Compression and Quality Assessment." *IEEE Transactions on Communications, Vol. COM-33.* IEEE. pp. 551-557. June, 1985.

Pennebaker, W.B., and J.L. Mitchell. *JPEG - Still Image Data Compression Standard.* Van Nostrand Reinhold. New York. 1993.

Rabbani, Majid and Paul W. Jones. *Digital Image Compression Techniques.* SPIE Optical Engineering Press. Bellingham, WA. 1991.

Reamer, Richard E. "United States Air Force Tactical Reconnaissance - An Analysis and Commentary." *SPIE Vol. 309, Airborne Reconnaissance V.* SPIE. Bellingham, WA. pp. 2-8. 1981.

Saaty, Thomas L. *The Analytic Hierarchy Process.* McGraw-Hill, Inc. New York. 1980.

Shapiro, Jerome M. "Embedded Image Coding using Zerotrees of Wavelet Coefficients." *IEEE Transactions on Signal Processing Vol. 41, No. 12.* pp. 3445-3462. 1993.

Wallace, Gregory K. "The JPEG Still Picture Compression Standard." *Communications of the ACM Vol. 34, No. 4.* April,1991.

Wilson, Andrew, ed. *Jane's Space Directory.* Jane's Information Group Ltd. Couldson, Surrey, UK.

Witten, Ian H., Radford M. Neal and John G. Cleary. "Arithmetic Coding for Data Compression." *Communications of the ACM.* ACM. pp. 520-540. June, 1987.

BIBLIOGRAPHY

_____. *Military Standard 188-198A - Joint Photographics Expert Group (JPEG) Image Compression for the National Transmission Format.* 1993.

_____. *National Imagery Transmission Format Standard (NITFS) Bandwidth Compression Study Phase IIIB Low Bit Rate Evaluation.* Eastman Kodak Company. Rochester, NY. 1994.

Adelson, Edward H. and Eero Simoncelli. "Orthogonal Pyramid Transforms for Image Coding." *SPIE Vol. 845, Visual Communications and Image Processing II.* SPIE. Bellingham, WA. pp. 50-58. 1987.

Allen, Phillip G. "Changing Reconnaissance Requirements." *SPIE Vol. 1342, Airborne Reconnaissance XIV.* SPIE. Bellingham, WA. pp. 18-23. 1978.

Antonini, Marc, Michel Barlaud, Pierre Mathieu and Ingrid Daubechies. "Image Coding using Wavelet Transform." *IEEE Transactions on Image Processing.* pp. 205-220. 1992.

Beser, Nicholas D. Class Notes, JHU Data and Image Compression (605.769) Fall 1993. Johns Hopkins University APL. 1993.

Beser, Nicholas D. "Image Data Compression Metrics." AIAA-93-4513-CP. AIAA. pp. 292-303. 1993.

Beser, Nicholas D. and A.A. Tomko. *Best of Breed Data Compression Evaluation Criteria.* Johns Hopkins University APL. Laurel, MD. 1994.

Beser, Nicholas D. "Space Data Compression Standards." *Johns Hopkins APL Technical Digest Vol. 15, No. 3.* Johns Hopkins University APL. Laurel, MD. pp. 206-223. 1994.

Boger, Dan and Carl Jones. Class Notes, NPS SS4002 Spring 1995. Naval Postgraduate School. 1995.

Brower, Bernard V. *The National Imagery Transmission Format Standard Bandwidth Compression Study Phase II Final Report.* Eastman Kodak Company. Rochester, NY. 1991.

Chen, Wen-Hsiung and William K. Pratt. "Scene Adaptive Coder." *IEEE Transactions on Communications, Vol. COM-32, No. 3.* IEEE. pp. 225-232. March, 1984.

Cherri, Abdallah K. and Mohammad A. Karim. "Optical Symbolic Substitution: Edge Detection using Prewitt, Sobel and Roberts Operators." *Applied Optics Vol. 28, No. 21.* Optical Society of America. pp. 4644-4648. November, 1989.

Cracknell, A.B. and L.W.B Hayes. *Introduction to Remote Sensing.* Taylor and Francis. London. 1991.

Elachi, Charles. *Introduction to the Physics and Techniques of Remote Sensing.* John Wiley and Sons. New York. 1987.

Eskicioglu, Ahmet M. "A Survey of Quality Measures for Gray Scale Image Compression." AIAA-93-4514-CP. AIAA. pp. 304-313. 1993.

Eskicioglu, Ahmet M., Paul S. Fisher and Siyuan Chen. "Image Quality Measures and their Performance." *1994 Space and Earth Science Data Compression Workshop.* National Aeronautics and Space Administration. Greenbelt, MD. pp. 55-67. 1994.

Eskicioglu, Ahmet M. and Paul S. Fisher. "The Variance of the Difference Image: An Alternative Quality Measure." *Proceedings of the International Picture Coding Symposium PCS '94.* The Center for Image Processing and Integrated Computing, CIPIC. UC Davis. pp. 88-91. 1994.

Farrelle, Paul M. *Recursive Block Coding for Image Data Compression.* Springer-Verlag. New York. 1990.

Fisher, Yuval. *Fractal Image Compression.* Springer-Verlag. New York. 1995.

Frigaard, Carsten. "Fast Fractal 2D/3D Image Compression." Institute of Electronic Systems. Aalborg University, Denmark. 1995.

Green, William F. "The Impact of Data Compression on Reconnaissance Systems." *SPIE Vol. 1342, Airborne Reconnaissance XIV.* SPIE. Bellingham, WA. pp. 261-268. 1990.

Gunston, Bill. *An Illustrated Guide to Spy Planes.* Prentice Hall Press. New York. 1983.

Habibi, Ali. "Survey of Adaptive Image Coding Techniques." *IEEE Transactions on Communications, Vol. COM-25, No. 11.* IEEE. pp. 1275-1284. November, 1977.

Hall, Charles F. "Subjective Evaluation of a Perceptual Quality Metric." *SPIE Vol. 310, Image Quality.* SPIE. Bellingham, WA. pp. 200-204. 1981.

Hilton, Michael L, Björn D. Jawerth and Ayan Sengupta. *Compressing Still and Moving Images with Wavelets.* 1994.

Howard, Paul G. and Jeffrey Scott Vitter. "Arithmetic Coding for Data Compression." *Proceedings of the IEEE, Vol. 82, No. 6.* IEEE. pp. 857-865. June, 1994.

Huffman, David A. "A Method for the Construction of the Minimum-Redundancy Codes." *Proceedings of the IRE.* pp. 1098-1101. September, 1952.

ISOA, APL. "TID 3.0 Documentation." ISOA, APL. April, 1995.

Latshaw, Gary L., Paul L. Zuzelo and S. James Briggs. "Tactical Photointerpreter Evaluations of Hardcopy and Softcopy Imagery." *SPIE Vol. 137, Airborne Reconnaissance III.* SPIE. Bellingham, WA. pp. 179-187. 1978.

Limb, John O. "Distortion Criteria of the Human Viewer." *IEEE Transactions on Systems, Man and Cybernetics, Vol. SMC-9, No. 12.* IEEE. pp. 778-793. 1979.

Max, Joel. "Quantizing for Minimum Distortion." *IRE Transactions on Information Theory.* pp. 7-12.

Mitchell, J.L. and W.B. Pennebaker. "Optimal Hardware and Software Arithmetic Coding Procedures for the Q-Coder." *IBM Journal of Research and Development, Vol. 32, No. 6.* International Business Machines Corporation. pp. 727-736. November, 1988.

Muolo, Michael J. *Space Handbook: A War Fighters Guide to Space.* Air University Press. Maxwell AFB, AL. 1993.

Murphy, Michael S. "Comparison of Transform Image Coding Techniques for Compression of Tactical Imagery." *SPIE Vol. 309, Airborne Reconnaissance V.* SPIE. Bellingham, WA. pp. 212-219. 1981.

Nelson, Mark. *The Data Compression Book.* M&T Books. 1991.

Nill, Norman B. "A Visual Model Weighted Cosine Transform for Image Compression and Quality Assessment." *IEEE Transactions on Communications, Vol. COM-33.* IEEE. pp. 551-557. June, 1985.

Pennebaker, W.B., J.L. Mitchell, G.G. Langdon, Jr. and R.B. Arps. "An Overview of the Basic Principle of the Q-Coder Adaptive Binary Arithmetic Coder." *IBM Journal of Research and Development, Vol. 32, No. 6.* International Business Machines Corporation. pp. 717-726. November, 1988.

Pennebaker, W.B. and J.L. Mitchell. "Probability Estimation for the Q-Coder." *IBM Journal of Research and Development, Vol. 32, No. 6.* International Business Machines Corporation. pp. 737-752. November, 1988.

Pennebaker, W.B., and J.L. Mitchell. *JPEG - Still Image Data Compression Standard.* Van Nostrand Reinhold. New York. 1993.

Pratt, William K. *Digital Image Processing.* John Wiley & Sons, Inc. New York. 1991.

Rabbani, Majid and Paul W. Jones. *Digital Image Compression Techniques.* SPIE Optical Engineering Press. Bellingham, WA. 1991.

Reamer, Richard E. "United States Air Force Tactical Reconnaissance - An Analysis and Commentary." *SPIE Vol. 309, Airborne Reconnaissance V.* SPIE. Bellingham, WA. pp. 2-8. 1981.

Saaty, Thomas L. *The Analytic Hierarchy Process.* McGraw-Hill, Inc. New York. 1980.

Sadowsky, John. "The Continuous Wavelet Transform: A Tool for Signal Investigation and Understanding." *Johns Hopkins APL Technical Digest, Vol. 15, No. 4.* Johns Hopkins APL. Laurel, MD. pp. 306-318. 1994.

Saghri, John A., Patrick S. Cheatham and Ali Habibi. "Image Quality Measure Based on a Human Visual System Model." *Optical Engineering, Vol. 28, No. 7.* SPIE. pp. 813-818. 1989.

Shapiro, Jerome M. "Embedded Image Coding using Zerotrees of Wavelet Coefficients." *IEEE Transactions on Signal Processing Vol. 41, No. 12.* pp. 3445-3462. 1993.

Vidakovic, Brani and Peter Müller. "Wavelets for Kids." Duke University. 1991.

Wallace, Gregory K. "The JPEG Still Picture Compression Standard." *Communications of the ACM Vol. 34, No. 4.* April,1991.

Wilson, Andrew, ed. *Jane's Space Directory 1993-1994.* Jane's Information Group Limited. Coulsdon, Surrey, UK. 1993.

Witten, Ian H., Radford M. Neal and John G. Cleary. "Arithmetic Coding for Data Compression." *Communications of the ACM.* ACM. pp. 520-540. June, 1987.

Zettler, William R., John Huffman and David C.P. Linden. "Application of Compactly Supported Wavelets to Image Compression." *AWARE Technical Report AD900119.* AWARE Inc. Cambridge, MA. 1990.

Zhuang, Yan and John S. Baras. "Optimal Wavelet Basis Selection for Signal Representation." *SPIE Vol. 2242, Wavelet Applications.* SPIE. pp. 200-211. 1994.

INITIAL DISTRIBUTION LIST

	Number of Copies
1. Defense Technical Information Center Cameron Station Alexandria, Virginia 22304-6145	2
2. Library, Code 52 Naval Postgraduate School Monterey, California 93943-5101	2
3. Chairman, Code SP Space Systems Academic Group Naval Postgraduate School Monterey, California 93943-5002	1
4. Dr. Terry Alfriend Space Systems Academic Group Code SP/AL Naval Postgraduate School Monterey, California 93943-5002	3
5. Captain Scott Thompson Office of the Chief of Naval Operations Code N63, Rom 4E679, The Pentagon Washington, DC 20350-2000	1
6. Commander, Naval Space Command ATTN: N112 5280 4th Street Dahlgren, Virginia 22448-5300	1
7. Dr. Nick Beser Johns Hopkins University Applied Physics Laboratory Johns Hopkins Road 23-328 Laurel, Maryland 20723-6099	3
8. Dr. Bruce Hammell Johns Hopkins University Applied Physics Laboratory Johns Hopkins Road Laurel, Maryland 20723-6099	1

9. Mr. L. James Happel — 1
   Johns Hopkins University Applied Physics Laboratory
   Johns Hopkins Road
   Laurel, Maryland 20723-6099

10. Captain LeGrow — 1
    Department of the Navy, CNO
    Code N632, Room 5P773, The Pentagon
    Washington, DC 20350-2000

11. Commander Jelinek — 1
    Department of the Navy, CNO
    Code N632, Room 5P773, The Pentagon
    Washington, DC 20350-2000

12. Lieutenant Mark A. Sanford, USN — 3
    Personnel Support Activity Detachment
    1 Amsterdam Road
    Scotia, New York 12302-9460